

REPORT DOCUMENTATION PAGE

AFRL-SR-AR-TR-05-

0434

The public reporting burden for this collection of information is estimated to average 1 hour per response, including gathering and maintaining the data needed, and completing and reviewing the collection of information. Send comments of information, including suggestions for reducing the burden, to Department of Defense, Washington Headquarters (0704-0188), 1215 Jefferson Davis Highway, Suite 1204, Arlington, VA 22202-4302. Respondents should be aware that subject to any penalty for failing to comply with a collection of information if it does not display a currently valid OMB control number.
PLEASE DO NOT RETURN YOUR FORM TO THE ABOVE ADDRESS.

1. REPORT DATE (DD-MM-YYYY) 20-09-2005		2. REPORT TYPE Final Report		3. DATES COVERED (From - To) June 2001 - June, 2005	
4. TITLE AND SUBTITLE Feedback Control Design for Counterflow Thrust Vectoring				5a. CONTRACT NUMBER	
				5b. GRANT NUMBER F49620-01-1-0550 01-0550	
				5c. PROGRAM ELEMENT NUMBER	
6. AUTHOR(S) Collins, Emmanuel G., Jr.				5d. PROJECT NUMBER	
				5e. TASK NUMBER	
				5f. WORK UNIT NUMBER	
7. PERFORMING ORGANIZATION NAME(S) AND ADDRESS(ES) Florida A&M University Division of Sponsored Programs 400 Foote Hilyer Administration Center Tallahassee, FL 32307					
9. SPONSORING/MONITORING AGENCY NAME(S) AND ADDRESS(ES) Air Force Office of Scientific Research 4015 Wilson Blvd., Rm. 213 Arlington, VA 22203 NM				10. SPONSOR/MONITOR'S ACRONYM(S) AFOSR/NM	
				11. SPONSOR/MONITOR'S REPORT NUMBER(S)	
12. DISTRIBUTION/AVAILABILITY STATEMENT Approved for public release; distribution unlimited					
13. SUPPLEMENTARY NOTES					
14. ABSTRACT Engineering research over the last few years has successfully demonstrated the potential of thrust vector control using counterflow at conditions up to Mach 2. Before this study, research had been limited to open-loop studies of counterflow thrust vectoring. For practical implementation it was vital that the counterflow scheme be used in conjunction with feedback control. Hence, the focus of this research was to develop and experimentally demonstrate a feedback control design methodology for counterflow thrust vectoring. This research focused on 2-D (pitch) thrust vectoring. The main goal was the design and implementation of robust controllers that yield closed-loop systems with fast response times, and avoid overshoot in order to aid in the avoidance of attachment. Additionally, these controllers should be simple and easy to implement and the methodology used to design them should be valid for the more difficult case of 3-D thrust vectoring, which leads to multiple-input, multiple-output control problems.					
15. SUBJECT TERMS Counterflow thrust vectoring, Robust Control, Aircraft propulsion, Fault detection and isolation					
16. SECURITY CLASSIFICATION OF:			17. LIMITATION OF ABSTRACT	18. NUMBER OF PAGES 76	19a. NAME OF RESPONSIBLE PERSON Emmanuel G. Collins, Jr.
a. REPORT	b. ABSTRACT	c. THIS PAGE			19b. TELEPHONE NUMBER (include area code) 850-410-6373

20051013 171

Table of Contents

1. Project Goals	3
2. Project Accomplishments	3
2.1 Feedback Control for Counterflow Thrust Vectoring with “Cold Flow”	3
2.2 Feedback Control for Counterflow Thrust Vectoring with a Turbine Engine ...	4
2.3 Robust Fault Detection and Isolation Using Robust ℓ_1 Estimation	7
Publications	7
Appendix A: “Design and Implementation of Feedback Control for Counterflow Thrust Vectoring”	
Appendix B: “Robust Fault Detection and Isolation Using Robust ℓ_1 Estimation”	

1. Project Goals

Engineering research over the last few years has successfully demonstrated the potential of thrust vector control using counterflow at conditions up to Mach 2. Flow configurations that include the pitch vectoring of rectangular jets and multi-axis vector control in diamond and axisymmetric nozzle geometries have been studied. Although bistable (on-off) fluid-based control has been around for some time, the present counterflow thrust vector control is unique because proportional and continuous jet response can be achieved in the absence of moving parts, while avoiding jet attachment, which renders most fluidic approaches unacceptable for aircraft and missile control applications. However, before this study, research had been limited to open-loop studies of counterflow thrust vectoring.

For practical implementation it was vital that the counterflow scheme be used in conjunction with feedback control. Hence, the focus of this research was to develop and experimentally demonstrate a feedback control design methodology for counterflow thrust vectoring.

This research focused on 2-D (pitch) thrust vectoring and addresses four key modeling issues. The first issue is to determine the measured variable to be commanded since the thrust vector angle is not measurable in real time. The second related issue is to determine the static mapping from the thrust vector angle to this measured variable. The third issue is to determine the dynamic relationship between the measured variable and the thrust vector angle. The fourth issue is to develop dynamic models with uncertainty characterizations.

The main goal was the design and implementation of robust controllers that yield closed-loop systems with fast response times, and avoid overshoot in order to aid in the avoidance of attachment. Additionally, these controllers should be simple and easy to implement and the methodology used to design them should be valid for the more difficult case of 3-D thrust vectoring, which leads to multiple-input, multiple-output control problems.

An additional objective of this research was the development of a robust fault detection and isolation methodology applicable to aircraft engines.

2. Project Accomplishments

Many of the project accomplishments are well documented in several publications [1-8]. Hence, this section briefly summarizes the main results and refers to the appropriate publications. Papers corresponding to these results are presented in the two appendices.

2.1 Feedback Control for Counterflow Thrust Vectoring with "Cold Flow"

This research considered feedback control for a counterflow thrust vectoring experiment located at the Fluid Mechanics Laboratory at the FAMU-FSU College of Engineering

(see Figure 1). The airflow in this experiment was ambient temperature, as opposed to the hot flow associated with implementation on an actual aircraft, and hence is termed "cold flow." A PID controller was developed for the system and was sometimes implemented with a Smith predictor and/or an anti-windup scheme. The performances of the PID controller, the PID controller with a Smith predictor, PID controller with anti-windup scheme, and PID with both the Smith predictor and anti-windup scheme were compared by both simulation and experimentation. Both simulation and experimental results demonstrated that PID controller with anti-windup was the most effective control scheme. The results were published in [2,4]. Reference [4] is given in Appendix A.

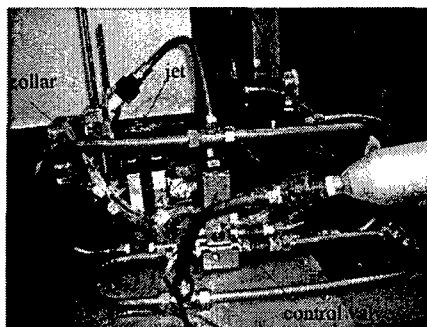


Figure 1. Counterflow Thrust Vector Control Experiment with "Cold Flow"

2.2 Feedback Control for Counterflow Thrust Vectoring with a Turbine Engine

This research considered feedback control for a counterflow thrust vectoring experiment involving a jet engine turbine (see Figure 2) located at the Portuguese Air Force Academy at Sintra, Portugal. This research required extensive experimental design as illustrated in Figures 3 thru 6, but enabled the experimentation to much more closely mimic flight conditions. PID controllers were designed using robust ℓ_1 theory based on mixed structured singular value theory in addition to several other more conventional tuning methods. As illustrated in Figures 7 and 8, good results were obtained with the robust ℓ_1 controller and its performance was very similar to the better-performing conventional tuning methods. However, the greatest advantage of robust ℓ_1 control design is that, unlike the conventional PID tuning methods, it extends to 3-D thrust vectoring, which results in a MIMO control design problem. The results of this research were published in a dissertation [5] and will soon be submitted to the *AIAA Journal.*, a very prestigious aerospace journal that publishes multidisciplinary papers.

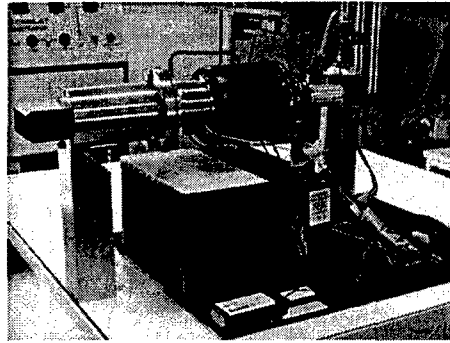


Figure 2. Artes Jet JG-100 Jet Engine Turbine Used in the Experiments

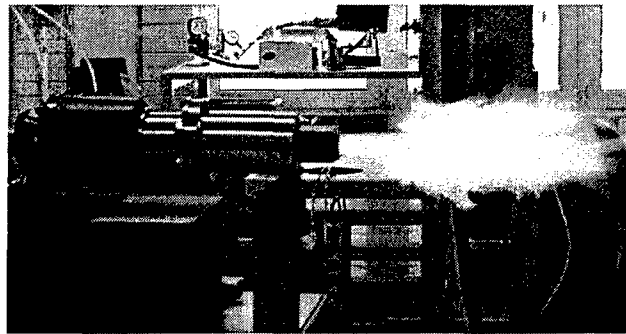


Figure 3. Early Engine Tests Showing Overheating

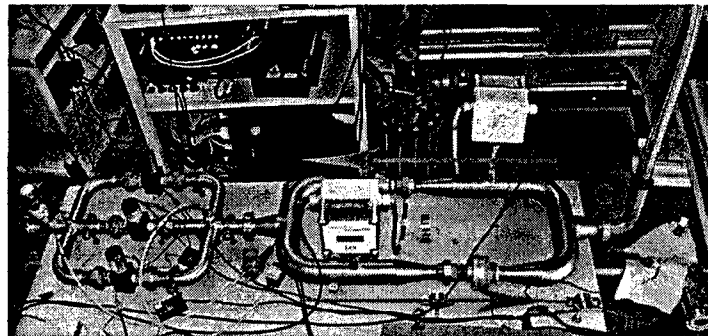


Figure 4. Counterflow Line Setup with Electronically Controlled Valves

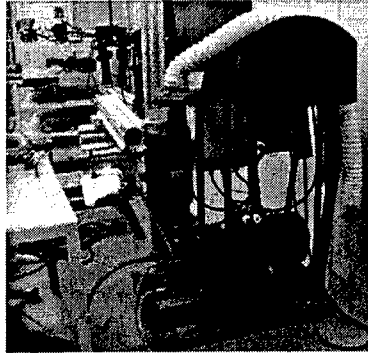


Figure 5. Vacuum Pump Used to Create the Counterflow

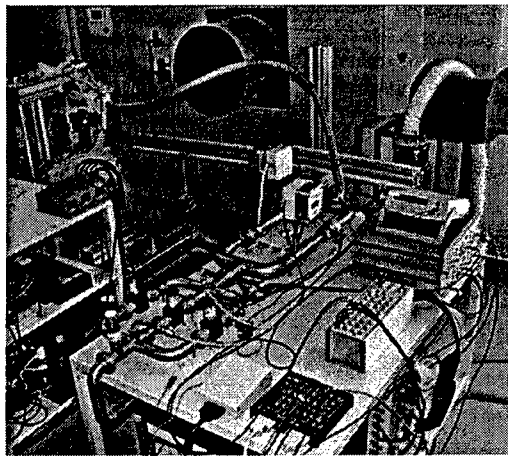


Figure 6. Experimental Setup with Electronically Controlled Valves

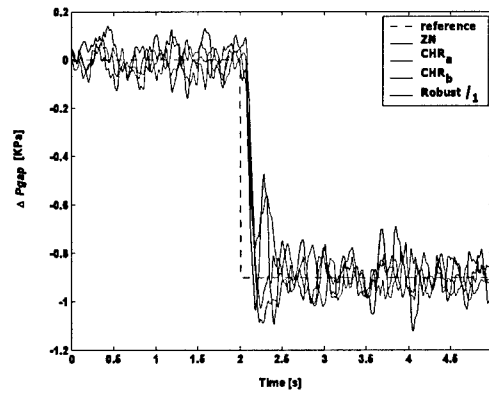


Figure 7. CFTV Closed Loop Step Response for P_{gap} from 0 KPa to -0.9 KPa (δ_v from 4.9 deg to 8.4 deg) Using Several PID Tuning Methods

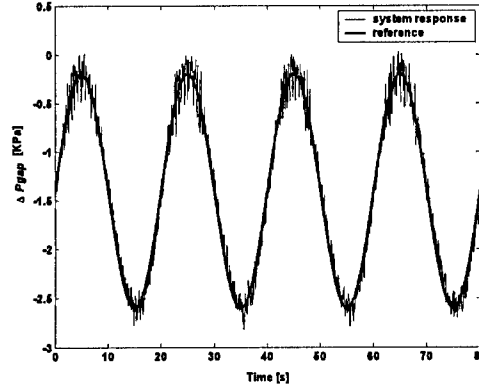


Figure 8. CFTV Closed Loop Sine Wave Response for Robust ℓ_1 Tuning Method

2.3 Robust Fault Detection and Isolation Using Robust ℓ_1 Estimation

This research considered the application of robust ℓ_1 estimation to robust fault detection and isolation. This was accomplished by developing a series, or bank, of robust estimators (full-order observers), each of which is designed such that the residual will be sensitive to a certain fault (or faults) while insensitive to the remaining faults. Robustness was incorporated by assuring that the residual remains insensitive to exogenous disturbances as well as modeling uncertainty. Mixed structured singular value and ℓ_1 theories were used to develop the appropriate threshold logic to evaluate the outputs of the estimators used for determining the occurrence and location of a fault. A real-coded genetic algorithm was used to obtain the estimator gain matrices. This approach to FDI was successfully demonstrated using a linearized model of a jet engine and was also applied to a complex, nonlinear benchmark problem. The results of this research were published in [1,3,7,8]. Reference [7] is given in Appendix B.

Publications

1. T. D. Curry and E. G. Collins, Jr., "Robust Fault Detection for a Jet Engine Using Robust ℓ_1 Estimation," *Proceedings of SAFEPROCESS 2003*, Washington, DC, June 2003.
2. E. G. Collins, Jr., Y. Zhao, F. Alvi, M. Alidu, and P. J. Strykowski, "Feedback Control for Counterflow Thrust Vectoring," *Proceedings of the American Control Conference*, Boston, MA, pp. 3654-3659, June 2004.
3. T. Curry and E. G. Collins, Jr., "Robust Fault Detection and Isolation Using Robust ℓ_1 Estimation," *Proceedings of the American Control Conference*, Boston, MA, pp. 2451-2456, June 2004.

4. Y. Zhao, E. G. Collins, Jr., F. Alvi, and D. Dores, "Design and Implementation of Feedback Control for Counterflow Thrust Vectoring," *AIAA Journal of Propulsion*, Vol. 21, No. 5, pp. 815-821, September-October 2005.
5. D. Dores, *Feedback Control for Counterflow Thrust Vectoring with a Turbine Engine: Experiment Design and Robust Control Design and Implementation*, Ph.D. Dissertation, Florida State University, Tallahassee, Florida, April 2005.
6. D. Dores, E. G. Collins, Jr., and F. Alvi, *Feedback Control for Counterflow Thrust Vectoring with a Turbine Engine*, in preparation for the *AIAA Journal*.
7. T. D. Curry and E. G. Collins, Jr., "Robust Fault Detection and Isolation Using Robust l_1 Estimation," *Journal of Guidance, Control, and Dynamics*, accepted.
8. T. D. Curry and E. G. Collins, Jr., "Application of Robust l_1 Fault Detection and Isolation to a Nonlinear Benchmark Diesel Engine Actuator," submitted to *Control Engineering Practice*.

**Appendix A: “Design and Implementation of Feedback Control
for Counterflow Thrust Vectoring” [4]**

Design and Implementation of Feedback Control for Counterflow Thrust Vectoring

Yanan Zhao*, Emmanuel G. Collins, Jr.†, Farrukh Alvi‡ and Delfim Dores§

Department of Mechanical Engineering
Florida A&M University - Florida State University
Tallahassee, FL 32310

Aircraft thrust vector control is currently implemented using movable control surfaces such as vanes and flaps. Counterflow thrust vectoring (CFTV) is a fluidic approach to thrust vectoring that has the potential to improve on the conventional approaches by reducing weight and increasing the reaction speed. Open-loop implementation of CFTV has been demonstrated in laboratory settings. However, ultimately this technology must be implemented using feedback control. The primary control objective is to achieve fast slew rates by compensating for the transportation delay and parameter uncertainties. The paper describes an experimental testbed for investigating feedback control of CFTV. System estimation results based on open-loop test data are presented. This paper then develops a PID control law, which is sometimes implemented with a Smith predictor to compensate for the transportation delay and/or an anti-windup scheme to compensate for actuator saturation. The control laws are experimentally demonstrated and their performance is compared using different types of reference signals.

*Research Associate

†John H. Seely Professor

‡Associate Professor. Member AIAA

§Ph.D. student

INTRODUCTION

The maneuverability of aircraft is traditionally achieved by the use of aerodynamic control surfaces such as ailerons, rudders, elevators and canards. The deflection of these surfaces modifies the exterior shape of the vehicle at critical points of its structure, thus creating a change in the aerodynamic forces acting on the vehicle and causing it to maneuver.^{1,2}

Thrust vector control (TVC) is a more recent technology that increases vehicle maneuverability by directly changing the direction of the thrust force vector. This approach has been successfully implemented on several military aircraft and has resulted in increased roll rates and enhanced maneuverability at low speed, high angle of attack flight conditions, where aerodynamic surfaces are very ineffective. TVC can also reduce the distance necessary for take off and landing or even make vertical take off and landing possible.

Current implementation of TVC employs movable control surfaces such as vanes and/or flaps arrayed around the nozzle exit to redirect the jet exhaust. The mechanical actuators and linkages used to change the thrust vector angle add weight and complexity to the aircraft, which leads to increased cost and maintenance requirements. In addition, the dynamic response of the jet is limited by the response of the mechanical actuators used and the thrust losses are not small.¹⁻³ A promising alternative approach is fluidic thrust vectoring, where secondary air flows are employed to redirect the primary jet. Fluidic thrust vectoring requires few or no moving parts in the primary nozzle; therefore it simplifies the hardware, and reduces weight and maintenance needs. In addition, it has the fast dynamic response inherent to fluidic devices.²⁻⁴

Counterflow thrust vectoring (CFTV) was first proposed by Strykowski and Krothapalli.⁵ It is a technique that is different than previously proposed fluidic techniques. Instead of having a secondary air stream inside the nozzle, CFTV uses a secondary flow travelling in the opposite direction to that of the primary jet outside the primary nozzle. Recent engineering research has successfully demonstrated the potential of thrust vector control using counterflow at conditions up to Mach 2.^{1,4,6} However, since fluidic concepts in general are bistable and hysteretic in nature, CFTV has some limitations. In particular, for certain CFTV geometries the primary jet tends to attach itself hysteretically to the suction collar at certain conditions. When this occurs, control of the thrust vectoring angle is lost. This *attachment* is difficult to overcome without large changes in flow conditions.³ A jet with a design Mach number 2 was used in this research because considerable experimental results are available to the authors at this Mach number. However, it should be noted that counterflow thrust vectoring has also been demonstrated at other Mach numbers, for example, Mach number 1.4 as well as for subsonic flow.^{2,6}

Past studies of CFTV have focused exclusively on the open-loop behavior. However, for

practical implementation it is vital that the counterflow scheme be used in conjunction with feedback. Hence, the primary objective of the research reported here is to design and implement effective feedback control laws for CFTV. Figure 1 illustrates that the CFTV feedback control loop constitutes an important minor loop of the overall aircraft attitude control. The control system must achieve fast slew rates by compensating for the transportation delay in the presence of significant parametric uncertainty. In addition, for certain CFTV geometries it must be able to compensate for the hysteresis that occurs when the counterflow is effectively stopped at attachment. Hysteresis is a nonlinearity for which traditional control methods are insufficient.⁷ However, CFTV can be continuously controlled over a wide range of operating conditions. Hence, in this paper control law design is developed assuming hysteresis does not occur. The design objective here is then to obtain fast slew rates in the presence of time delay and parametric uncertainty.

PID control and its variations (P, PI or PD) is the most commonly used control law in process control applications for the compensation of both delayed and non-delayed processes.⁸ PID controllers often display robustness to incorrect process model order assumptions and limited process parameter changes. As the detailed physics of CFTV system are not entirely understood, a PID controller was developed based on a model estimated using experimental open-loop data. A Smith predictor was used in conjunction with PID control to compensate for the effects of time delay while an anti-windup scheme was used to compensate for actuator saturation.

The paper is organized as follows. Section 2 describes some of the details of the CFTV concept along with the experimental testbed developed for feedback control development. Section 3 presents system modelling and analysis results. Section 4 develops a PID control law and shows how it can be used in conjunction with a Smith predictor and/or an anti-windup scheme and then gives some closed-loop simulation results. Section 5 presents experimental results. Finally, Section 6 presents some conclusions.

DESCRIPTION OF COUNTERFLOW THRUST VECTORING (CFTV) AND THE EXPERIMENTAL TESTBED

In this section, the concept of CFTV is described and an experimental testbed for investigating feedback control of CFTV is presented.

Counterflow Thrust Vectoring

The basic geometry of a CFTV device used for pitch vectoring is illustrated in Figure 2. The collars are placed on either side of the primary flow nozzle (top and bottom in the figure) creating gaps between the exhaust jet and the collar surfaces which are curved away

from the jet axis in the streamwise direction. To achieve upward thrust vectoring at an angle δ_v , for example, a secondary counterflow must be established between the primary jet and the upper collar surface, creating a continuous flow path between the surrounding ambient fluid and the vacuum system. The action of counterflow in the upper shear layer gives rise to asymmetric entrainment and a cross-stream pressure gradient sufficient to vector the jet.⁴ When the vacuum system is activated, creating counterflow in the gap between the jet and the collar, continuous thrust vectoring can be achieved.⁴ Previous experimental studies have demonstrated continuous control for values of δ_v up to 20 degrees.² In this figure, G represents the gap height and H is the nozzle height.

It is important to recognize that the thrust vectoring angle cannot be directly measured in practical implementation of CFTV, although experimental techniques do allow its measurement in laboratory settings. However, it has been shown that the pressure parameter $\frac{\Delta P_G A_{side}}{\rho U^2 A_{jet}}$, which is essentially a non-dimensional ratio of the side force acting on the collar and the axial force imposed by the jet, has a nearly linear relationship to the thrust vector angle over a wide range of conditions (see Figure 9 of the reference paper).⁴ Here, P_G is the pressure established in the secondary stream as measured in the jet exit plane on the collar surface, ΔP_G is the static negative gauge pressure in the jet exit plane on the collar surface (i.e., $\Delta P_G = P_{atm} - P_G$, where P_{atm} represents the absolute atmospheric pressure), A_{side} is the collar side area, ρ is the primary jet density, U is the primary jet velocity, and A_{jet} is the jet area at the nozzle exit. Thus, in practice ΔP_G will be selected as the command variable.

For certain CFTV geometries, if the pressure on the collar wall drops too much (i.e., ΔP_G becomes very large), the deflection of the jet will be too severe and it will attach to the wall. If this happens, continuous control of the jet is compromised since at this time thrust vectoring angle would generally jump to a value near the collar terminal angle. Jet attachment is a hysteretic phenomenon since once the jet is attached to the collar, changes in the secondary flow have little effect on the thrust vectoring angle, and simply reducing the counterflow rate to reduce ΔP_G back to the value at which jet attachment occurred is not sufficient to release the jet from the collar.³ Feedback control of CFTV in the presence of hysteresis is beyond the scope of this paper.

Experimental Testbed

To investigate feedback control of CFTV, a testbed has been successfully set up in the Fluid Mechanics Research Laboratory at the Florida A&M University - Florida State University College of Engineering. The characteristics of the current experiment have been shown to match those in the literature.^{2,4}

The experimental testbed consisted of five major parts: a jet, a collar, a control valve, two

pumps and the pipe connections. A schematic functional diagram of the testbed is shown in Figure 3. Notice that for simplicity only one collar was used. Hence, the experiment allows only positive pitch angles δ_v .

The rectangular Mach 2 jet in the exit plane has a width of 32.5 mm and a height of 5 mm. The inner contour of the collar is an arc of constant radius of curvature swept through an angle α and extending downstream of the nozzle exit for a distance given by $L = R \sin \alpha$, where $L = 34$ mm, $R = 78.5$ mm and $\alpha = 25.6$ deg (see Figure 4).

The forward stream to the jet is supplied by a high-displacement reciprocating compressor, which is capable of supplying air at a maximum storage pressure of 160 bars. The vacuum source for the counterflow is provided by two Fuji VFC804A-7W pumps mounted downstream of the test rig. The two pumps can be connected in series as shown in Figure 3, or they can be used separately, i.e., either of the pumps can be disconnected from the testbed.

To implement feedback control, a control valve is installed between the collar and pumps to control the counterflow, which determines the thrust vector angle. A model 27N pneumatic R-DDV servovalve from HR Textron is used in the test rig for this purpose.

Data acquisition and control are implemented using dSPACE, which consists of a DS2002 A/D board, a DS2102 D/A board, a DS1005 PPC board, and a PX10 expansion box. To monitor the jet pressure (which should be 115 psi for a Mach 2 jet), a Validyne multiple range pressure transducer (model DP15TL) is used. There are 11 static pressure taps along the collar wall, and the multiple pressure measurements required to determine the collar static pressure distribution are facilitated by a Scanivalve model OED2 pressure sampling scanner.

SYSTEM MODELLING AND ANALYSIS

Although the general principles responsible for CTFV, i.e., increased entrainment due to counterflow are known (see reference^{1,4} for details), the detailed physics of CFTV are not entirely understood; thus it is difficult to build a CFTV model using first principles. In this section, system modelling and parameter estimation were performed based on open-loop tests.

Open-loop tests and system modelling

The model required for feedback control design has the voltage to the control valve as the input and the command variable ΔP_G as the output. To study the system characteristics under different operating regions, the CFTV testbed has been extensively tested for step inputs with amplitude 1 volt, 2 volts, \dots , 5 volts. (The range of the control valve voltage

is [0, 5] volts.) To capture the transient performance of the system clearly, the step signals were applied at $t = 10$ sec. One set of resulting step responses is shown in Figure 5.

The tests were performed with both the first and second vacuum pumps on and a geometry ratio of $G/H = 0.38$. The sampling rate was chosen as $T_s = 0.01$ sec. Due to the installation of collar at the exit of jet engine, thrust vectoring exists with even a fully closed control valve. To consider only the effect of the control valve, open-loop response curves representing $-(P_G(t > 10\text{sec}) - P_G(t = 10\text{sec}))$ were plotted as shown in Figure 6. A negative sign is used since a higher control valve signal always results in lower gap pressure along the collar.

By observing the open-loop step responses of the system, second order models were constructed to represent the system dynamics. The second order models with time delay are of the form, $\frac{K}{T^2s^2 + 2T\xi s + 1}e^{-Ls}$, where K is the gain, T is the time constant, ξ is the damping ratio, and L is the time delay of the system. Experimental open-loop methods for parameter estimation have been widely studied.⁹ A method proposed by Huang and Chou,¹⁰ a five-point method, was used to estimate the process parameters. The estimated parameters under five different control valve voltage inputs are listed in Table 1.

Figure 7 compares the simulated step responses based on the estimated models and the test data under different control valve voltages. It is seen that a second order plus time delay model closely matches the time delay and the steady state. However, the estimated model has a slightly faster rise time than the test data since the dashed lines in Figure 7 arrive at their steady-state values slightly faster than the solid lines.

As shown in Table 1, under different control valve inputs, the parameters of the second order models had different values. The gain K varied within 13.06% of its average value, the time constant T varied within 15.84% of its average value, the damping ratio ξ varied within 5.93% of its average value, and the time delay L varied within 2.82% of its average value. The parametric variations at different operating points are assumed to be due to nonlinearities in the control valve and fluid dynamics.

Additional Sources of Uncertainty in the CFTV System

The CFTV system suffers from additional sources of uncertainty. Two of the major sources are described below.

The dynamics of CFTV changes along with the power level of the pumps. For example, the running temperature of the pumps affects their efficiency, and thereafter the CFTV dynamics. A colder pump is more efficient and hence produces higher counterflow. Usually, the gap pressure obtained with a colder pump is lower than that of a warmer pump. An inter-cooling system is desired to keep the pump running at peak efficiency; however, it is

not used in the current experiment.

The dynamics of CFTV also changes along with ambient conditions. For example, the temperature of the air supplied to the jet affects the performance of CFTV system. The air source of the compressor is the atmosphere air. Due to the variation of atmospheric temperature, the temperature of the air supplied to the jet engine is not guaranteed. The temperature change causes the performance variation of the primary flow, and thereafter the collar pressure.

Another set of open-loop tests was performed to illustrate the above uncertainty. It was also conducted with both the first and second vacuum pumps on and a geometry ratio of $G/H=0.38$ as was the case corresponding to the tests of Table 1. However, though not explicitly recorded, the ambient temperature for this set was different. (This test set was conducted on the afternoon of April 14, 2004, while the test set corresponding to Table 1 was conducted on the morning of March 3, 2004.) In addition, the power level of the pumps varied for the two experiments. The gains obtained with the second experiment are shown in Table 2. It is seen that these values are significantly different from those shown in Table 1.

PID Controller Design

After the CFTV system model was obtained, feedback control laws were designed to control ΔP_G and thus the counterflow thrust vector angle δ_v . To increase the ability to maneuver the vehicle quickly, one control objective is to have a fast slew rate. In addition, to ensure smooth motion, it is desired to avoid system overshoot. These objectives must be accomplished in the presence of substantial parametric variation and system delay. Control valve saturation is also a significant obstacle. PID controllers are the most commonly used controllers in industrial practice.⁸ PID control was used here due to its simple structure, ease of design and robustness under certain model and parameter uncertainties. A Smith predictor was used along with PID control to compensate for the system delay. An anti-windup strategy was used to compensate for actuator saturation.

PID Control Using Tuning Rules

Many PID tuning rules are available for second order system with time delay.¹¹ A direct synthesis method proposed by Miluse etc.¹¹ was used to obtain the PID gains. For 0% overshoot, the proportional gain, the integral time constant and derivative time constant of the PID controller can be computed as $K_p = 0.736 \frac{\xi T}{KL}$, $T_i = 2\xi T$, and $T_d = 0.5T/\xi$.

In the first design attempt, the variation of the system dynamics was neglected, and only one PID controller was designed for the entire operating region of the system. Thus the model parameters were taken as the average of the corresponding parameters as given in Table 1.

The gains of the obtained PID controller are $K_p = 2.0615$, $K_i = 1.9872$, and $K_d = 0.7106$. The controller demonstrated its robustness during experimental implementation.

Smith Predictor

As described above, open-loop system tests revealed the existence of transportation delay in the CFTV system. A Smith predictor is an effective tool for compensating for system time delay. As shown in Figure 8, the basic idea of the Smith predictor is to use a delay free model of the process dynamics G_m to predict the effect of current control actions on the actual delayed process output. Additional feedback from the actual process output is then used to compensate for modelling error and process disturbances.¹²⁻¹⁴ Here, the primary controller used in the Smith predictor is the PID controller designed above.

Note that the Smith predictor is very dependent on the system model. To cope with the process parameter variation, an adaptive Smith predictor using on-line parameter estimation or robust tuning is preferred.^{12,14} In the current implementation, G_m is taken as the average dynamics model.

Antiwindup

The working range of the control valve is within [0 5] volts. It was observed that for the PID controller, control valve saturation occurred at higher setpoints where the generated control signal was higher than 5 volts. Saturation also occurred at the instant of dramatic setpoints change, where a big change of control signal was produced to track the change of setpoint. In addition, saturation occurred in the case of abnormal sensor noise.

The performance of PID control can be severely deteriorated in practical cases by the presence of saturation of the actuators, which causes the well-known phenomenon of integrator windup, leading to large overshoot, slow settling time, and, sometimes, even instability in the system.¹⁵ The traditional method to deal with the integrator windup problem is to tune the PID controller ignoring the actuator saturation and subsequently to add an anti-windup compensator to prevent the degradation of performance.¹⁵⁻¹⁷

One of the commonly used approaches is back-calculation (or tracking anti-windup).^{16,17} As shown in Figure 9, this approach consists of recomputing the integral term once the controller saturates. In particular, the integral value is reduced by feeding back the difference of the saturated u_s and unsaturated control signal u . Here T_i is the tracking time constant, and its value determines the rate at which the integral term is reset; its choice determines the performances of the overall control scheme. Some suggestions are to set $T_i = T_i$, but in some cases higher values may give further improvement in performance.^{16,17}

Simulation Results

Simulations were performed with four different control approaches, i.e., PID, PID with Smith prediction, PID with anti-windup, and PID with both Smith prediction and anti-windup. The average model obtained for PID control law design was used in the simulation. As discussed above, the thrust vector angle cannot be directly measured in a practical implementation of CFTV. In the present study, the corresponding vector angles are estimated based on the nearly linear relation between the thrust vector angle and the gap pressure such as that shown in Figure 9 of the reference paper.⁴ This relationship is used here since it is based on extensive test results, which demonstrate that this pressure value is a reliable predictor of the vector angle. Since the pressure distributions along the collar obtained in the present test setup matched well with that of the reference paper, the use of the previously established correlation is well-justified. Consequently, the uncertainty associated with the present vector angles is estimated to be similar to that associated with previous measurements in reference,⁴ and is approximately ± 0.5 degrees. The comparison of the controller performance was conducted under two cases: 1) without controller saturation, and 2) with controller saturation.

In the first case, the CFTV system had a setpoint of 13.75 psi (corresponding to a 5.0 deg vector angle). In this case, anti-windup had no effect because all the generated signals were within the working range of the control valve (i.e., [0 5] volts). As shown in Figure 10, the control signal generated from the PID controller overlapped with that of the PID controller with the anti-windup scheme, and the control signal generated from the Smith predictor overlapped with the PID controller with both the Smith predictor and the anti-windup scheme. Likewise, as shown in Figure 11, the output signal resulting from the PID controller overlapped with that of the PID controller with the anti-windup scheme, and the output signal of the Smith predictor overlapped with PID controller with both the Smith predictor and the anti-windup scheme. Since the control signal generated by the Smith predictor was less aggressive than the corresponding PID controller, the Smith predictor did not cause overshoot and the transient performance is smoother than the corresponding PID controller.

As an example of the second case, the CFTV system tracked a setpoint change from 14.3 psi to 12.6 psi (corresponding to an increase of thrust vector angle from 2.0 deg to 9.2 deg). Controller saturation occurred due to the dramatic change of the setpoint, and the higher targeted setpoint at 12.6 psi. Figure 12 shows the generated control signal after the change of setpoint at 5 sec. As shown in the figure, the control signal generated by the PID controller was above 5 volts over most of the time period, the control signal generated by the PID controller with the Smith predictor was smaller but went beyond 5 volts after 9.2 sec.

Anti-windup had the ability to avoid controller saturation; as shown in the figure, the control signals generated by the PID controller with the anti-windup scheme and the PID controller with both the Smith predictor and the anti-windup scheme were less or equal to 5 volts. The simulation was conducted with $1/T_t = 6/T_i$. It was observed that the higher the value of $1/T_t$, the stronger the anti-windup to avoid controller saturation. The simulated controller performance in Figure 13 shows that with the current choice of T_t , the Smith predictor was less aggressive than the corresponding PID anti-windup controller.

In the simulation results the Smith predictor did not show the desired advantage over the PID controller in compensating for the time delay and producing faster response times. The major reason for this is that the said to have a dominant time delay if $L \geq 5T$.¹⁸ Simulations were conducted with increased time delay (e.g., L was increased to twice its original value), and it was seen that for PID control the longer time delay yielded a smaller phase margin which led to large overshoot and very oscillatory behavior. For large enough time delay (e.g. when the time delay was five times its original value for the CFTV system) the system became unstable. However, the performance of the Smith predictor was consistent as the time delay increased.

Experimental Results

Extensive experiments with the four different control approaches were conducted and the performances of the different approaches were compared. Here, the experimental results under two types of reference signals are given.

In the case of a pulse reference signal, the desired collar gap pressure is 12.6 psi (corresponding to 9.2 deg thrust vector angle) from 0 to 20 sec, 14.0 psi (corresponding to 3.7 deg thrust vector angle) from 20 to 40 sec, and it is 13.0 psi (corresponding to 8.0 deg thrust vector angle) from 40 to 60 sec. Figure 14 compares experimental outputs with different control approaches. Here both the dramatic changes of reference signal (from 12.6 psi to 14.0 psi, and from 14.0 psi to 13.0 psi) and the higher setpoint (12.6 psi) led to high control signal demands; thus the PID controller always exhibited overshoot. The PID controller with the Smith predictor was always less aggressive, producing no overshoot while having a slower rise time than the PID controller alone. The PID controller with the anti-windup scheme had the ability to remove the overshoot while obtaining a similar rise time to that of the PID controller alone; here $T_t = T_i$ was used. The PID controller with both the Smith predictor and anti-windup scheme was less aggressive than the PID controller with the Smith predictor or the PID controller with the anti-windup, having a slower rise time.

In the case of a sine wave reference signal, the desired collar gap pressure is described by $P_{gap} = 0.85\sin(0.1\pi t + \pi/2) + 13.45$, corresponding to a maximum thrust vector angle

of 9.2 deg and a minimum thrust vector angle of 2.0 deg. Figure 15 compares experimental outputs with different control approaches. Here, due to the continuous reference signal, control saturation occurred only when the reference signal was around 12.6 psi (where the generated control signal was lighter above 5 volts) and 14.3 psi (where the generated control signal was slightly below 0 volt). The PID controller with anti-windup was very close to the PID controller except around the instants of peak point 12.6 psi and 14.3 psi. The PID controller with the Smith predictor was less aggressive and had a slower response than the corresponding PID controller. The PID controller with both the Smith predictor and anti-windup scheme was very close to the PID controller with the Smith predictor. In all the four cases, the closed-loop response exhibited obvious delay in tracking the reference signal. For example, the delay time for the PID controller to the reference sine wave signal was about 1.3 sec.

In all of the experimental results, the four types of controllers demonstrated performance similar to the simulation results. In general, PID control with a Smith predictor eliminated the overshoot of the PID controller but increased the rise time and did not avoid controller saturation. PID control with anti-windup was effective in the presence of controller saturation. PID control with both a Smith predictor and anti-windup scheme did not show an advantage over PID control with only anti-windup. One reason for this is that, as discussed above, for a system such as CFTV that is not time delay dominant, a Smith predictor shows little or no advantage. In addition, a Smith predictor is model-based, and the estimated model may be significantly different from the true CFTV model.

A PID controller with anti-windup is preferred in the current controller design. Extensive experimental results demonstrated the robustness of the PID controller under system uncertainties. However to further improve the system performance, an adaptive scheme which can update the system parameters and control parameters online should be investigated.

CONCLUSIONS

Counterflow thrust vectoring control is a promising technique for aircraft engine attitude control. Feedback control of CFTV is needed to obtain desired thrust vector angles by compensating for the transportation delay and parameter uncertainties.

This paper has described an experimental testbed for investigating feedback control of CFTV. System modelling was achieved using open-loop test data. A PID controller was developed for the system and was sometimes implemented with a Smith predictor and/or an anti-windup scheme. Then the performances of the PID controller, the PID controller with the Smith predictor, the PID controller with the anti-windup scheme, and the PID controller with both the Smith predictor and the anti-windup scheme were compared by both simulation

and experimentation. Both simulation and experimental results demonstrated that the PID controller with anti-windup was the most effective control scheme.

This paper studied feedback control of one dimensional CFTV where only the pitch vectoring was considered. Open-loop, three dimensional CFTV has been demonstrated in a laboratory setting. Feedback control of the three dimensional CFTV will result in a multivariable control problem and hence is significantly more difficult than the corresponding single-input, single-output control problem considered here. The multivariable case will be studied in future research.

Acknowledgments

The authors would like to thank the U.S. Air Force Office of Scientific Research (Contract F49620-01-0550) for financial support this research. We also thank Robert Avant, Fritz Dittus and Mohammed I. Alidu for helping in the experimental setup.

References

- ¹Alvi, F. S., Strykowski, P. J., Krothapalli, A., and Forliti, D. J., "Vectoring Thrust in Multiaxies Using Confined Shear Layers," *ASME Journal of Fluids Engineering*, Vol. 122, 2000, pp. 3-13.
- ²Maria, M., "Experimental Study on Counter-flow Thrust Vector Control of a Subsonic Rectangular Nozzle," Florida State University Technical Report, 2000.
- ³Flamm, J. D., "Experimental Study of a Nozzle Using Fluidic Counterflow for Thrust Vectoring," AIAA Paper 98-3255, 1998.
- ⁴Strykowski, P. J., Krothapalli, A., and Forliti, D. J., "Counterflow Thrust Vectoring of Supersonic Jets," *AIAA Journal*, Vol. 34, 1996, pp. 2306-2314.
- ⁵Strykowski, P. J. and Krothapalli, A., "The Countercurrent Mixing Layer: Strategies for Shear-Layer Control," AIAA Paper 93-3260, 1993.
- ⁶M. R. Van der Veer, "Counterflow Thrust Vectoring of a Subsonic Rectangular Jet," M.S. Thesis, University of Minnesota, Minneapolis, MN, 1995.
- ⁷Su, C. Y., Stepanenko, Y., Svoboda, J., and Leung, T. P., "Robust Adaptive Control of a Class of Nonlinear Systems with Unknown Backlash-like Hysteresis," *IEEE Transactions on Automatic Control*, Vol. 45, No. 12, 2000, pp. 2427-2432.
- ⁸Astrom, K. J. and Hagglund, T., "The Future of PID Control," *Control Engineering Practice*, Vol. 9, No. 11, 2001, pp. 1163-1175.
- ⁹O'Dwyer, A., "The Estimation and Compensation of Process with Time Delays," Ph.D Thesis, Dublin City University, Ireland, 1996.

¹⁰Huang, C. T. and Chou, C. J., "Estimation of the Underdamped Second-order Parameters from the System Transient," *Industrial and Engineering Chemistry Research*, Vol. 33, No. 1, 1994, pp. 174-176.

¹¹O'Dwyer, A., "PI and PID Controller Tuning Rules for Time Delay Processes: A Summary," Dublin Institute of Technology Technical Report AOD-00-01, 2000.

¹²Lee, D. K., Lee, M. Y., Sung, S. W., and Lee, I. B., "Robust PID Tuning for Smith Predictor in the Presence of Uncertain," *Journal of Process Control*, Vol. 9, No. 1, 1999, pp. 79-85.

¹³Aziz, K. I. and Thomson, M., "Minimal Controller Synthesis for Time-delay Systems Using a Smith Predictor," *IEE Colloquium on Adaptive Controllers in Practice - Part Two, London, UK*, 1996, pp. 4/1 - 4/5.

¹⁴Hang, C. C. and Chong, B. W., "On Methods of Treating dc levels in an Adaptive Digital Smith Predictor," *IEEE Transactions on Automatic Control*, Vol. 35, No. 1, 1990, pp. 65-66.

¹⁵Shin, H. B., "New Anti-windup PI Controller for Variable-Speed Motor Drives," *IEEE Transactions on Industrial Electronics*, Vol. 45, No. 3, 1998, pp. 445-450.

¹⁶Visioli, A., "Modified Anti-windup Scheme for PID Controllers," *IEE Proceedings - Control Theory Application*, Vol. 150, No. 1, 2003, pp. 49-54.

¹⁷Bohn, C. and Atherton, D. P., "An Analysis Package Comparing PID Anti-windup Strategies," *IEEE Control System Magazine*, Vol. 15, No. 2, 1995, pp. 34-40.

¹⁸Rad, A. B., Tsang, K. M., and Lo, W. L., "Adaptive Control of Dominant Time Delay Systems via Polynomial Identification," *IEE Proceedings - Control Theory and Applications*, Vol. 142, No. 5, 1995, pp. 433-438.

List of Table Captions

Table 1: Model estimation at different input values

Table 2: Gains obtained with another set of open-loop test data

Input Amplitude (volts)	K	T (sec)	ξ	L (sec)
1	0.2889	0.6681	0.9181	0.5440
2	0.3258	0.5089	0.8650	0.5543
3	0.3365	0.5033	0.8504	0.5730
4	0.3501	0.6420	0.8626	0.5458
5	0.3602	0.6675	0.8372	0.5694
Average Value	0.3323	0.5980	0.8667	0.5573

TABLE 1:

Input Amplitude (volts)	K
1	0.3500
2	0.3352
3	0.3171
4	0.3232
5	0.3401
Average	0.3331

TABLE 2:

List of Figure Captions

- Figure 1: Aircraft attitude control using fluidic thrust vector control
- Figure 2: Schematic of counter-flow thrust vector control
- Figure 3: Schematic functional diagram of the testbed
- Figure 4: The collar
- Figure 5: Open-loop step responses under different control valve voltage
- Figure 6: Converted open-loop step responses under different control valve voltage
- Figure 7: Comparison of test response (solid line) and system estimated response (dashed line)
- Figure 8: Block diagram of a Smith predictor
- Figure 9: Block diagram of an anti-windup Smith predictor
- Figure 10: Simulated controller performance at setpoint 13.75 psi: generated control signal
- Figure 11: Simulated controller performance at setpoint 13.75 psi: output signal
- Figure 12: Generated controller signal from setpoint 14.3 psi to 12.6 psi: 5 to 20 sec
- Figure 13: Simulated controller performance from setpoint 14.3 psi to 12.6 psi
- Figure 14: Controller performance under a pulse reference signal
- Figure 15: Controller performance under a sine wave reference signal

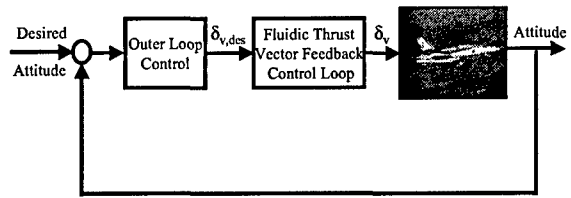


FIGURE 1:

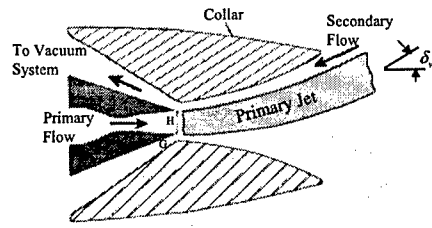


FIGURE 2:

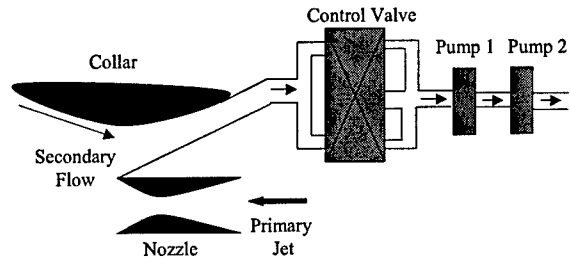


FIGURE 3:

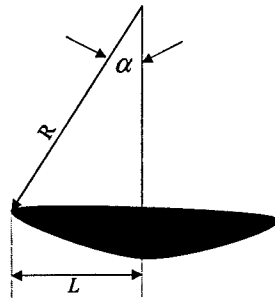


FIGURE 4:

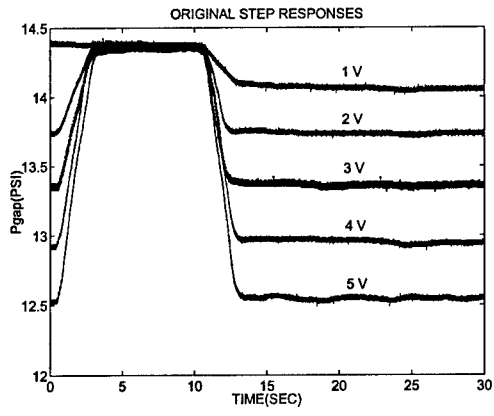


FIGURE 5:

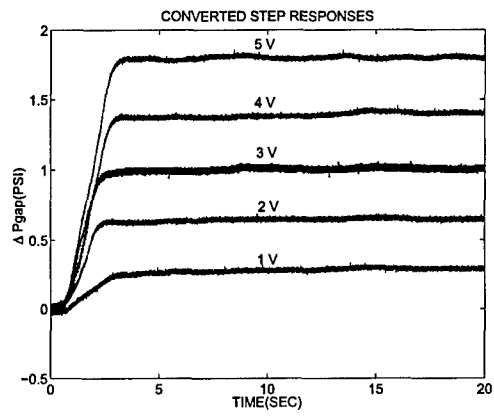


FIGURE 6:

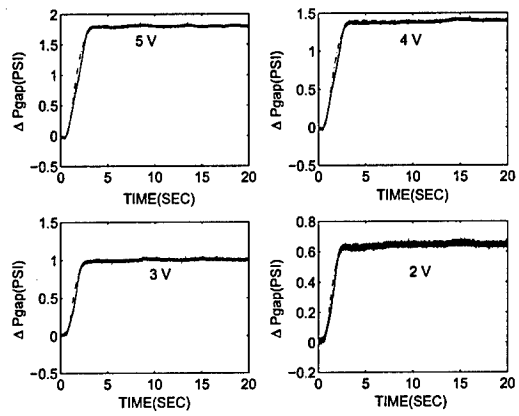


FIGURE 7:

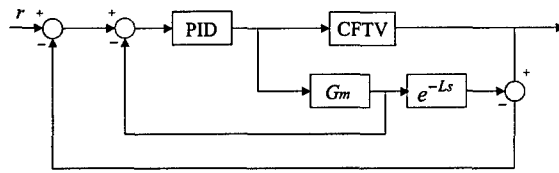


FIGURE 8:

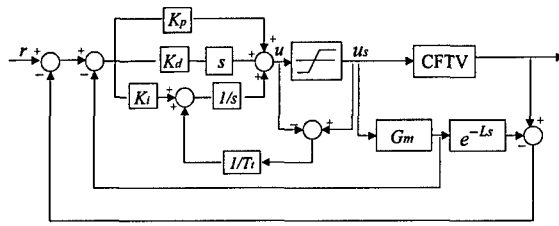


FIGURE 9:

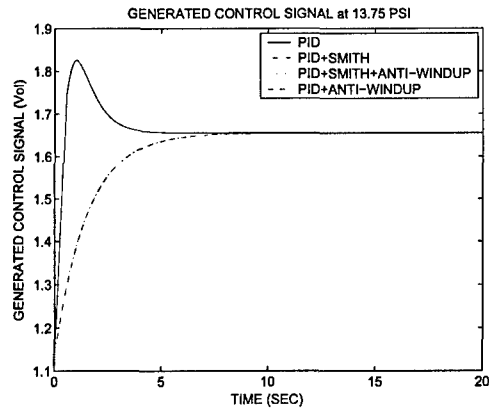


FIGURE 10:

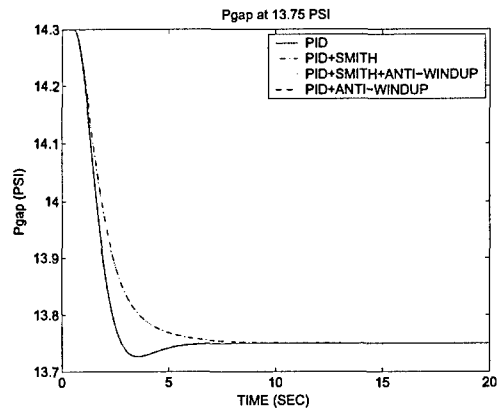


FIGURE 11:

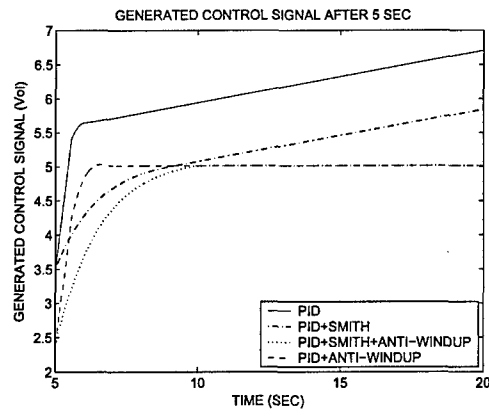


FIGURE 12:

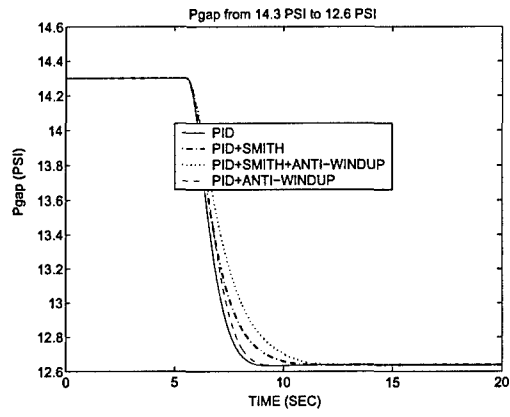


FIGURE 13:

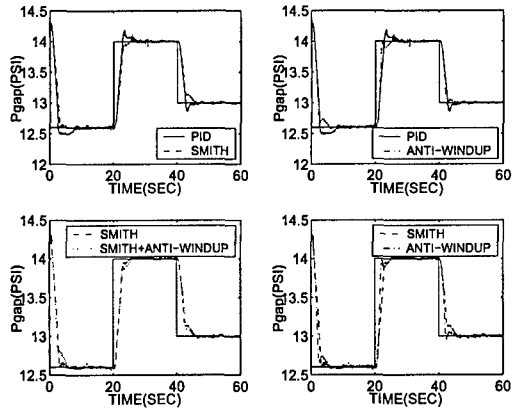


FIGURE 14:

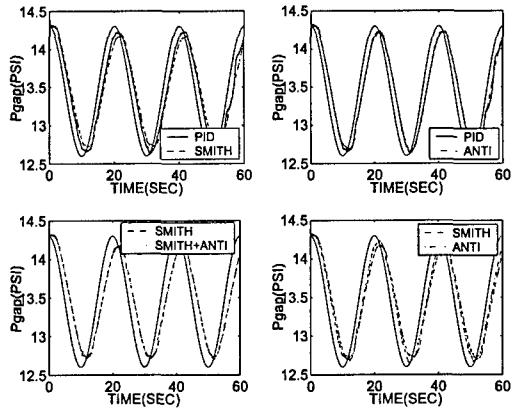


FIGURE 15:

Appendix B: “Robust Fault Detection and Isolation Using Robust l_1 Estimation” [7]

Robust Fault Detection and Isolation Using Robust ℓ_1 Estimation

Tramone D. Curry* and Emmanuel G. Collins, Jr.*

Florida A&M University-Florida State University, Tallahassee, FL 32310

Abstract

This paper considers the application of robust ℓ_1 estimation to robust fault detection and isolation. This is accomplished by developing a series, or bank, of robust estimators (full-order observers), each of which is designed such that the residual will be sensitive to a certain fault (or faults) while insensitive to the remaining faults. Robustness is incorporated by assuring that the residual remains insensitive to exogenous disturbances as well as modeling uncertainty. Mixed structured singular value and ℓ_1 theories are used to develop the appropriate threshold logic to evaluate the outputs of the estimators used for determining the occurrence and location of a fault. A real-coded genetic algorithm is used to obtain the estimator gain matrices. This approach to FDI is successfully demonstrated using a linearized model of a jet engine.

*FAMU-FSU College of Engineering, Department of Mechanical Engineering

Nomenclature

$\mathcal{R}, \mathcal{C}, \mathcal{Z}^+$	real numbers, complex numbers, nonnegative integers
$\mathcal{R}^{m \times n}, \mathcal{C}^{m \times n}$	$m \times n$ real matrices, complex matrices
$\mathcal{D}^n, \mathcal{N}^n, \mathcal{P}^n$	$n \times n$ real diagonal, nonnegative definite, positive definite matrices
$0, I$	zero matrix, identity matrix
tr	trace
$M_2 > M_1$	$M_2 - M_1$ positive definite
$M_2 \geq M_1$	$M_2 - M_1$ nonnegative definite
$\dim(M)$	dimension of M
$\ z(\cdot)\ _{\infty, 2}$	$\text{ess sup}_{t \geq 0} \ z(t)\ _2$
$\ z(\cdot)\ _{(\infty, 2), [N_0, N]}$	$\text{ess sup}_{t \in [N_0 T, NT]} \ z(t)\ _2$
$\ H_{zw}\ _1$	$\sup_{w(\cdot) \in \ell_\infty} \frac{\ z\ _{\infty, 2}}{\ w\ _{\infty, 2}}$
z_{ij}	(i, j) element of matrix Z
$\text{Vec}(Z), Z \in \mathcal{R}^{m \times n}$	$[z_{11}, \dots, z_{m1}, z_{12}, \dots, z_{m2}, \dots, z_{mn}]^T$
$\text{diag}(Z), Z \in \mathcal{D}^n$	$[z_{11}, z_{22}, \dots, z_{nn}]^T$

Introduction

In modern systems such as aircraft and spacecraft, there is an increasing demand for reliability and safety. For example, a jet engine is very critical for an aircraft and if faults occur, the consequences can be extremely serious.¹ Many dynamic systems are complex technical systems that involve extensive use of multiple sensors, actuators and other system components, any one of which could fail or deteriorate. Hence, health monitoring and supervision of these systems is essential for the improvement of reliability, safety and dependability of operations. This entails continuously checking a physical system for faults and taking appropriate actions to maintain the operation in such situations. In particular, the objective is to detect and isolate failures or anomalies in the sensors, actuators and components.

One of the primary approaches to model-based, fault detection and isolation uses state or output estimators.²⁻⁸ Detection of a fault is achieved by comparing the actual behavior of the plant to that expected on the basis of the model; deviations are indications of a fault (or disturbances, noise or modeling errors).⁹ Fault isolation can be achieved by dedicating an estimator such that the residual is sensitive to only one particular fault. In particular, referring to Figure 1, a bank of estimators is used to generate residuals $r(t)$. These residuals are then analyzed by some appropriate logic (e.g., logic based on thresholds or fuzzy logic)

which infers whether faults have occurred (fault detection) and where they have occurred (fault isolation).

In many approaches to the FDI problem the robustness aspect is commonly introduced in relation to the fault detection.¹⁰ The estimators shown in Figure 1 may be designed in a variety of ways, for example by using Kalman filter theory (i.e., H_2 optimal estimation),¹¹⁻¹³ H_∞ theory,¹⁴⁻¹⁶ or ℓ_1 theory.¹⁷⁻¹⁹ Whichever method is used for designing the estimator, it will use an idealized mathematical description of the underlying plant. In practice this model of the plant is never totally accurate, which can degrade the quality of the residuals produced by the estimators. The errors in the plant model may be either parametric or unstructured (e.g., unmodeled dynamics). To reduce the degradation in the quality of the residuals upon which the FDI process is based, and hence to reduce the false alarm rate, it is imperative that the plant uncertainty be explicitly taken into account in the design of the estimators.

Until recent work,^{11,14,18,20} the relatively nonconservative mixed structured singular value (MSSV) techniques²¹⁻²⁴ had not been applied to robust estimation, although more conservative techniques, based on the small gain theorem or fixed quadratic Lyapunov functions, had been used.^{15,16,25-27} Conservatism in robustness theory involves how the theory actually models the uncertainty. For example, even if the uncertainty is real and parametric, the small gain theorem assumes that the uncertainty is complex and unstructured. Likewise, fixed quadratic Lyapunov function theory assumes that the uncertainty is arbitrarily time-varying. MSSV theory, which considers both parametric uncertainty and unmodelled dynamics, allows real parametric uncertainty to be treated as slowly time-varying, real parametric uncertainty, which is a much less conservative model. The reduced conservatism allows the estimators to be used for more accurate fault detection. Specifically, the fixed thresholds are smaller, allowing the detection of smaller faults. With more conservative theories the thresholds are larger, causing some smaller faults to go undetected. Although the example in this paper focuses exclusively on sensor faults the theory is developed to include actuator faults as well.

This paper considers the application of robust ℓ_1 estimation to fault robust fault detection and isolation. This is accomplished by developing a series, or bank, of robust estimators (full-order observers), each of which is designed such that the residual will be sensitive to a certain fault (or faults) while insensitive to the remaining faults. Robustness is incorporated by assuring that the residual remains insensitive to exogenous disturbances as well as modelling uncertainty. Mixed structured singular value and ℓ_1 theories are used to develop the appropriate threshold logic to evaluate the outputs of the estimators used for determining the occurrence and location of a fault. A real-coded genetic algorithm is used to obtain the

estimator gain matrices. The effectiveness of this robust FDI technique is illustrated as it is applied to a discrete-time, linear uncertain model of an advanced afterburning turbofan engine.

The organization of this paper is as follows. Section 2 presents the formulation of the closed-loop uncertain system to which estimation will be applied. The application of robust ℓ_1 estimation to robust fault detection and isolation is presented in Section 3. Section 4 discusses results of an illustrative example of a jet engine, while Section 5 gives concluding remarks.

Robust ℓ_1 Estimation

Consider a discrete-time, linear uncertain dynamic system

$$x(k+1) = (A + \Delta A)x(k) + Bu(k) + D_{\infty,1}w_{\infty}(k), \quad k \in \mathcal{Z}^+ \quad (1)$$

$$y(k) = (C + \Delta C)x(k) + Du(k) + D_{\infty,2}w_{\infty}(k), \quad (2)$$

$$z(k) = E_{\infty}x(k), \quad (3)$$

where $x \in \mathcal{R}^n$ is the state vector, $u \in \mathcal{R}^d$ is the control input, $y \in \mathcal{R}^p$ denotes the plant measurements, $z \in \mathcal{R}^q$ is the performance output to be estimated, and $w_{\infty} \in \mathcal{R}^{d_{\infty}}$ denotes an ℓ_{∞} disturbance signal satisfying $\|w_{\infty}(\cdot)\|_{\infty,2} \leq 1$. The uncertainties ΔA , ΔB and ΔC satisfy

$$\Delta A \in \mathcal{U}_A \triangleq \{\Delta A \in \mathcal{R}^{n \times n} : \Delta A = -H_A F_A G_A, \quad F_A \in \mathcal{F}_A\}, \quad (4)$$

$$\Delta C \in \mathcal{U}_C \triangleq \{\Delta C \in \mathcal{R}^{p \times n} : \Delta C = -H_C F_C G_C, \quad F_C \in \mathcal{F}_C\}, \quad (5)$$

where

$$\mathcal{F}_A \triangleq \{F_A \in \mathcal{D}^r : M_{A,1} \leq F_A \leq M_{A,2}\}, \quad (6)$$

$$\mathcal{F}_C \triangleq \{F_C \in \mathcal{D}^t : M_{C,1} \leq F_C \leq M_{C,2}\}, \quad (7)$$

with $M_{A,1}, M_{A,2} \in \mathcal{D}^r$, $M_{C,1}, M_{C,2} \in \mathcal{D}^t$, $M_{A,2} - M_{A,1} \geq 0$, and $M_{C,2} - M_{C,1} \geq 0$.

It is desired to design a full-order observer of the form

$$x_e(k+1|k) = A_e x_e(k|k-1) + (B - WD)u(k) + W[y(k) - Cx_e(k|k-1)] \quad (8)$$

to estimate the state vector x , where $W \in \mathcal{R}^{n \times p}$ and $A_e \in \mathcal{R}^{n \times n}$ are the parameters to be determined.

The state estimation error is defined as

$$e(k) \triangleq x(k) - x_e(k|k-1), \quad (9)$$

which using (1), (2), and (8) can be shown to obey the evolution equation

$$e(k+1) = (A_e - WC)e(k) + (A - A_e + \Delta A - W\Delta C)x(k) + (D_{\infty,1} - WD_{\infty,2})w_{\infty}(k). \quad (10)$$

Now define the error output $\tilde{z} \in \mathcal{R}^{q_p}$ as $\tilde{z}(k) \triangleq E_{\infty}e(k)$. Then augmenting (1) with (10) yields

$$\tilde{x}(k+1) = (\tilde{A} + \Delta\tilde{A})\tilde{x}(k) + \tilde{D}_1w_{\infty}(k), \quad (11)$$

$$\tilde{z}(k) = \tilde{E}\tilde{x}(k), \quad (12)$$

where

$$\begin{aligned} \tilde{x}(k) &= \begin{bmatrix} x(k) \\ e(k) \end{bmatrix}, \quad \tilde{A} = \begin{bmatrix} A & 0 \\ A - A_e & A_e - WC \end{bmatrix}, \\ \tilde{D}_1 &= \begin{bmatrix} D_{\infty,1} \\ D_{\infty,1} - WD_{\infty,2} \end{bmatrix}, \quad \tilde{E} = \begin{bmatrix} 0 & E \end{bmatrix}. \end{aligned} \quad (13)$$

Furthermore, $\Delta\tilde{A}$ satisfies

$$\Delta\tilde{A} \in \tilde{\mathcal{U}}_A \triangleq \{\Delta\tilde{A} \in \mathcal{R}^{2n \times 2n} : \Delta\tilde{A} = -\tilde{H}_A\tilde{F}_A\tilde{G}_A, \tilde{F}_A \in \tilde{\mathcal{F}}_A\}, \quad (14)$$

$$\tilde{\mathcal{F}}_A \triangleq \{\tilde{F}_A \in \mathcal{D}^{r+t} : M_1 \leq \tilde{F}_A \leq M_2\}, \quad (15)$$

where

$$\tilde{F}_A = \begin{bmatrix} F_A & 0 \\ 0 & F_C \end{bmatrix}, \quad \tilde{H}_A = \begin{bmatrix} H_A & 0 \\ H_A & -WH_C \end{bmatrix}, \quad \tilde{G}_A = \begin{bmatrix} G_A & 0 \\ G_C & 0 \end{bmatrix}, \quad (16)$$

and

$$M_1 = \text{diag}(M_{A,1}, M_{C,1}), \quad M_2 = \text{diag}(M_{A,2}, M_{C,2}). \quad (17)$$

The robust ℓ_1 estimation problem is to find the estimator parameters A_e and W such that the combined system (8), (11)-(12) is asymptotically stable and the cost functional

$$\mathcal{J}(W) = \|H_{zw}\|_1^2, \quad (18)$$

is minimized, where H_{zw} is the convolution operator from the disturbance $w_\infty(\cdot)$ to the ℓ_∞ performance variable $\tilde{z}(\cdot)$.

As shown in,²⁸ direct minimization of the ℓ_1 norm can lead to irrational estimators. However, Haddad et. al.²⁹ shows it is possible to characterize an upper bound on the ℓ_1 performance. For some uncertainty set $\mathcal{U} \subset \mathcal{R}^{n \times n}$, $\Delta A \in \mathcal{U}$, $x \in \mathcal{R}^n$, $z \in \mathcal{R}^q$ $w_\infty(\cdot) \in \mathcal{R}^{d_\infty}$, the ℓ_1 performance bound as a function of $\Delta \tilde{A}$ is given in the following proposition

Proposition 1 *Let $\alpha > 1$ and assume there exists a positive-definite matrix $Q_{\Delta A}$ satisfying*

$$Q_{\Delta \tilde{A}} = \alpha(\tilde{A} + \Delta \tilde{A})Q_{\Delta \tilde{A}}(\tilde{A} + \Delta \tilde{A})^T + \frac{\alpha}{\alpha - 1}V_\infty, \quad (19)$$

where $V_\infty \triangleq \tilde{D}_1 \tilde{D}_1^T$. Then $\tilde{A} + \Delta \tilde{A}$ is asymptotically stable. Furthermore, the ℓ_1 norm of the convolution operator H_{zw} from disturbances $w(\cdot)$ to the performance variable $\tilde{z}(\cdot)$ satisfies the bound

$$\|H_{zw}\|_1^2 \leq \sup_{\Delta \tilde{A} \in \mathcal{U}} [\text{tr}(\tilde{E}Q_{\Delta \tilde{A}}\tilde{E}^T)]^{\frac{1}{q}}, \quad \Delta \tilde{A} \in \mathcal{U}. \quad (20)$$

If, in addition, α is chosen such that $\sqrt{\alpha}(\tilde{A} + \Delta \tilde{A})$ is asymptotically stable, then the existence of a positive-definite solution $Q_{\Delta \tilde{A}}$ is guaranteed.

Proof. Follows from Lemma in.¹⁸

Remark 1 *Minimization of the upper bound is a more appropriate approach than some conventional methods. Typical linear programming methods³⁰ that seek to directly minimize the ℓ_1 norm do not allow a fixed architecture estimator or controller design. These methods normally result in very high order estimators or controllers, which are not practical for implementation.*

In order to obtain an upper bound on the ℓ_1 performance $\|H_{zw}\|_1^2$ over the entire uncertainty set \mathcal{U} , a multiplier framework will be used to bound $Q_{\Delta \tilde{A}}$ for all $\Delta A \in \mathcal{U}$ where

$$\mathcal{U} \triangleq \{\Delta \tilde{A} \in \mathcal{R}^{2n \times 2n} : \Delta \tilde{A} = -H_0 F G_0, \quad F \in \mathcal{F}\}. \quad (21)$$

Let $G(z) \in \mathcal{C}^{q \times d_\infty}$ be the transfer function representation of the system described in (11) and (12). The Popov-Tsytkin multiplier^{11,14,18,24} has the transfer function form

$$M(z) = H + N \frac{z - 1}{z}, \quad (22)$$

where $H \in \mathcal{D}^m$, $N \in \mathcal{D}^m$ ($m = r + t$) with $H > 0$ and $N \geq 0$. Let A_a denote the state matrix of the augmented system $M(z)G(z)$. Then, the uncertain system for robust analysis

is given by³¹

$$x_a(k+1) = (A_a + \Delta A_a)x_a(k) + D_{a,\infty}w_\infty(k), \quad (23)$$

$$z(k) = E_a x_a(k), \quad (24)$$

where $x_a(k) = [x_m^T(k)x^T(k)]^T$, $x_m(k) \in \mathcal{R}^m$ denotes the states of the multiplier,

$$A_a = \begin{bmatrix} 0 & 0 \\ H_0 & \tilde{A} \end{bmatrix}, \quad D_{a,\infty} = \begin{bmatrix} 0 \\ D_\infty \end{bmatrix}, \quad E_a = \begin{bmatrix} 0 & E \end{bmatrix}, \quad (25)$$

and

$$\Delta A_a \in \mathcal{U}_a \triangleq \{\Delta A_a \in \mathcal{R}^{m+n} : \Delta A_a = -H_a F G_a, \quad F \in \mathcal{F}\}, \quad (26)$$

where

$$H_a = \begin{bmatrix} 0 \\ H_0 \end{bmatrix}, \quad G_a = \begin{bmatrix} 0 & G_0 \end{bmatrix}. \quad (27)$$

Note that the uncertainty set \mathcal{U} in (21) is a subset of \mathcal{U}_a . The next theorem provides an upper bound for the ℓ_1 performance for all $\Delta A_a \in \mathcal{U}_a$.

Theorem 1 *Let $\alpha > 1$, $q \geq 1$. Suppose there exists $H \in \mathcal{P}^n$, $N \in \mathcal{N}^n$ and $Q_a \geq 0$ such that $2H(M_2 - M_1)^{-1} - G_a Q_a G_a^T > 0$, and Q_a satisfies the algebraic Riccati equation*

$$\begin{aligned} Q_a = & \alpha(A_a - H_a M_1 G_a)Q_a(A_a - H_a M_1 G_a)^T + [\sqrt{\alpha}(A_a - H_a M_1 G_a)Q_a C_a^T - \sqrt{\alpha}B_a(H + N) \\ & + S_a N][2H(M_2 - M_1)^{-1} - G_a Q_a G_a^T]^{-1}[\sqrt{\alpha}(A_a - H_a M_1 G_a)Q_a C_a^T - \sqrt{\alpha}B_a(H + N) \\ & + S_a N]^T + \frac{\alpha}{\alpha - 1}V_{a,\infty}, \end{aligned} \quad (28)$$

where $V_{a,\infty} \triangleq D_{a,\infty}D_{a,\infty}^T$ and $S_a \triangleq \begin{bmatrix} I \\ 0 \end{bmatrix}$, where $\dim(S_a) = \dim(H_a)$.

Then,

$$\{(A_a + \Delta A_a), [\frac{\alpha}{\alpha - 1}V_{a,\infty}]^{\frac{1}{2}}\} \text{ is stabilizable, } \Delta A_a \in \mathcal{U}, \quad (29)$$

if and only if $(A_a + \Delta A_a)$ is asymptotically stable for each $\Delta A_a \in \mathcal{U}_a$ and in this case, the ℓ_1 performance $\|H_{zw}\|_1^2$ is bounded as

$$\|H_{zw}\|_1^2 \leq [\text{tr}(E_a Q_a E_a^T)]^{\frac{1}{q}}, \quad \Delta A_a \in \mathcal{U}_a. \quad (30)$$

Proof. The proof can be completed in the same manner as proof to results in.²³

Robust FDI Using Robust ℓ_1 Estimation

Now consider the fault driven system

$$x(k+1) = (A + \Delta A)x(k) + Bu(k) + D_{\infty,1}w_{\infty}(k) + R_a f_a(k), \quad (31)$$

$$y(k) = (C + \Delta C)x(k) + D_p u(k) + D_{\infty,2}w_{\infty}(k) + R_s f_s(k), \quad (32)$$

$$z(k) = E_{\infty}x(k), \quad (33)$$

where $f_a \in \mathcal{R}^{r_a}$ and $f_s \in \mathcal{R}^{r_s}$ are the actuator and sensor fault vectors, respectively. The fault distribution matrices R_a and R_s are assumed to be known. Defining $f \triangleq [f_a^T \ f_s^T]^T$ yields the modified system

$$x(k+1) = (A + \Delta A)x(k) + Bu(k) + D_{\infty,1}w_{\infty}(k) + R_1 f(k), \quad (34)$$

$$y(k) = (C + \Delta C)x(k) + D_{\infty,2}w_{\infty}(k) + R_2 f(k), \quad (35)$$

$$z(k) = E_{\infty}x(k), \quad (36)$$

where

$$R_1 = \begin{bmatrix} R_a & 0 \end{bmatrix}, \quad R_2 = \begin{bmatrix} 0 & R_s \end{bmatrix}. \quad (37)$$

Equations (34)-(35) can be written in the expanded forms

$$x(k+1) = (A + \Delta A)x(k) + Bu(k) + D_{\infty,1}w_{\infty}(k) + R_{1,1}f_1(k) + \dots + R_{1,g}f_g(k), \quad (38)$$

$$y(k) = (C + \Delta C)x(k) + D_{\infty,2}w_{\infty}(k) + R_{2,1}f_1(k) + \dots + R_{2,g}f_g(k), \quad (39)$$

where $R_{1,i}$ (respectively, $R_{2,i}$) denotes the i^{th} column of the matrix R_1 (respectively, R_2). Let $g \triangleq r_a + r_s$. For $i \in \{1, 2, \dots, g\}$ the term $f_i(k)$ represents the i^{th} individual fault of $f(k)$ and $R_{1,i}$ (respectively, $R_{2,i}$) represents its directional characteristics. Assume that $f_i(k)$ is the "target fault," i.e., the fault that it is desired to detect. Without loss of generality, the vector of "nuisance faults", representing the faults that are *not* to be detected (by the robust fault detection filter), is given by $\bar{f}_i \triangleq [f_1(k) \cdots f_{i-1}(k) \ f_{i+1}(k) \cdots f_g(k)]$. Hence, (38)-(39) can be replaced by

$$x(k+1) = (A + \Delta A)x(k) + Bu(k) + D_{\infty,1}w_{\infty}(k) + R_{1,i}f_i(k) + \bar{R}_{1,i}\bar{f}_i(k), \quad (40)$$

$$y(k) = (C + \Delta C)x(k) + D_{\infty,2}w_{\infty}(k) + R_{2,i}f_i(k) + \bar{R}_{2,i}\bar{f}_i(k). \quad (41)$$

Define $\tilde{w} \triangleq [w^T \bar{f}_i^T]^T$. Then, (40) and (41) can be written as a set of systems

$$\Sigma_i \begin{cases} x(k+1) = (A + \Delta A)x(k) + Bu(k) + D_1\tilde{w}(k) + R_{1,i}f_i(k), \\ y(k) = Cx(k) + D_2\tilde{w}(k) + R_{2,i}f_i(k), \\ z(k) = E_\infty x(k) \end{cases} \quad (42)$$

where

$$D_1 = \begin{bmatrix} D_{\infty,1} & \bar{R}_{1,i} \end{bmatrix}, \quad D_2 = \begin{bmatrix} D_{\infty,2} & \bar{R}_{2,i} \end{bmatrix}. \quad (43)$$

It is desired to design a bank of full-order observers (corresponding to each faulty system) described in (8) to estimate the performance output $E_\infty x(k)$. As previously stated, $A_e \in \mathcal{R}^{n \times n}$ and $W \in \mathcal{R}^{n \times p}$ are the parameters to be determined. (Typically, one chooses $E_\infty = C$ such that z corresponds to the noise and fault free output associated with the measurement y .) Detection of a fault is achieved by comparing the actual behavior of the plant to the the output of the estimators; deviations are indications of a fault (or disturbances, noise or modeling errors).

Let the residual error be defined as

$$r(k) \triangleq P[y(k) - Cx_e(k|k-1) - Du(k)], \quad (44)$$

where the $g \times p$ gain matrix P^{32} is chosen such that r has a fixed direction when responding to the target fault. Fault isolation can be achieved by designing an estimator such that estimation error (i.e. the residual) is sensitive to only one particular fault. Specifically, each is designed to be sensitive to a particular fault and insensitive to the remaining faults. In addition, these estimators are made robust against exogenous disturbances and modeling uncertainties. Referring to Figure 1, the bank of estimators is used to generate residuals $r(k)$. These residuals are then analyzed by some appropriate logic (e.g., logic based on thresholds) which infers whether faults have occurred (fault detection) and where they have occurred (fault isolation).

Using (42), the state estimation error in (9) can be shown to obey the evolution equation

$$\begin{aligned} e(k+1) = & (A_e - WC)e(k) + (A + \Delta A - W\Delta C - A_e)x(k) \\ & + (D_1 - WD_2)w_\infty(k) + (R_{1,i} - WR_{2,i})f_i(k). \end{aligned} \quad (45)$$

Augmenting (42) with (45) yields

$$\tilde{x}(k+1) = (\tilde{A} + \Delta\tilde{A})\tilde{x}(k) + \tilde{D}_1 w_\infty(k) + \tilde{R}_1 f_i(k), \quad (46)$$

$$\tilde{z}(k) = \tilde{E}\tilde{x}(k), \quad (47)$$

where

$$\begin{aligned} \tilde{x}(k) &= \begin{bmatrix} x(k) \\ e(k) \end{bmatrix}, \quad \tilde{A} = \begin{bmatrix} A & 0 \\ A - A_e & A_e - WC \end{bmatrix}, \\ \tilde{D}_1 &= \begin{bmatrix} D_1 \\ D_1 - WD_2 \end{bmatrix}, \quad \tilde{R}_1 = \begin{bmatrix} R_{1,i} \\ R_{1,i} - WR_{2,i} \end{bmatrix}, \quad \tilde{E} = \begin{bmatrix} 0 & E_\infty \end{bmatrix}. \end{aligned} \quad (48)$$

Let J_{rw} represent the ℓ_1 norm of the system operator from the disturbance vector \tilde{w} to the residual r and let J_{rf} represent the ℓ_1 norm of the system operator from the target fault f_i to the residual r . Following previous derivations, it is possible to characterize upper bounds \mathcal{J}_{rw} and \mathcal{J}_{rf} such that

$$J_{rw} = \|H_{rw}\|_1^2 \leq \mathcal{J}_{rw}, \quad (49)$$

$$J_{rf} = \|H_{rf}\|_1^2 \leq \mathcal{J}_{rf}. \quad (50)$$

Using multiplier theory, the uncertain system is given by

$$x_a(k+1) = (A_a + \Delta A_a)x_a(k) + D_{a,w}\tilde{w}(k) + D_{a,f}f_i(k), \quad (51)$$

$$\tilde{z}(k) = E_a x_a(k), \quad (52)$$

where $x_a(k) = [x_m^T(k) \tilde{x}^T(k)]^T$ and $x_m(k) \in \mathcal{R}^m$ is as previously described. The ℓ_1 performance functions then have the bounds,

$$\mathcal{J}_{rw}(A_e, W, P, H, N) = [\text{tr}(E_a Q_{a,w} E_a^T)^q]^{\frac{1}{q}}, \quad (53)$$

$$\mathcal{J}_{rf}(A_e, W, P, H, N) = [\text{tr}(E_a Q_{a,f} E_a^T)^q]^{\frac{1}{q}}, \quad \Delta A_a \in \mathcal{U}_a, \quad (54)$$

where $Q_{a,w}$ and $Q_{a,f}$ satisfy the algebraic Riccati equations

$$\begin{aligned} Q_{a,w} = & \alpha(A_a - H_a M_1 G_a)Q_{a,w}(A_a - H_a M_1 G_a)^T + [\sqrt{\alpha}(A_a - H_a M_1 G_a)Q_{a,w}C_a^T \\ & - \sqrt{\alpha}H_a(H + N) + S_a N][2H(M_2 - M_1)^{-1} - G_a Q_{a,w}G_a^T]^{-1}[\sqrt{\alpha}(A_a - H_a M_1 G_a)Q_{a,w}C_a^T \\ & - \sqrt{\alpha}H_a(H + N) + S_a N]^T + \frac{\alpha}{\alpha - 1}V_{a,w}, \end{aligned} \quad (55)$$

$$\begin{aligned} Q_{a,f} = & \alpha(A_a - H_a M_1 G_a)Q_{a,f}(A_a - H_a M_1 G_a)^T + [\sqrt{\alpha}(A_a - H_a M_1 G_a)Q_{a,f}C_a^T \\ & - \sqrt{\alpha}H_a(H + N) + S_a N][2H(M_2 - M_1)^{-1} - G_a Q_{a,f}G_a^T]^{-1}[\sqrt{\alpha}(A_a - H_a M_1 G_a)Q_{a,f}C_a^T \\ & - \sqrt{\alpha}H_a(H + N) + S_a N]^T + \frac{\alpha}{\alpha - 1}V_{a,f}, \end{aligned} \quad (56)$$

where $V_{a,w} \triangleq D_{a,w}D_{a,w}^T$, $V_{a,f} \triangleq D_{a,f}D_{a,f}^T$, and $S_a \triangleq \begin{bmatrix} I \\ 0 \end{bmatrix}$, with $\dim(S_a) = \dim(H_a)$.

Robust FDI filter design may be approached by choosing A_e , W and P such that \mathcal{J}_{rw} is small and \mathcal{J}_{rf} is large.¹ A minimization problem that expresses this objective is

$$\min_{A_e, W, P} \mathcal{J} = \beta \mathcal{J}_{rw} + (1 - \beta) \frac{1}{\mathcal{J}_{rf}} + \gamma \frac{\mathcal{J}_{rw}}{\mathcal{J}_{rf}}, \quad (57)$$

where $\beta \in [0, 1]$ and $\gamma > 0$ are arbitrarily chosen weighting scalars. With an enforced stability constraint, this optimization problem can be solved using a real-coded genetic algorithm, as discussed in the next section.

Now consider the set of uncertain, discrete-time systems

$$x(k+1) = (A + \Delta A)x(k) + D_1 w_\infty(k) + R_{1,i} f_i(k), \quad (58)$$

$$y(k) = Cx(k) + D_2 w_\infty(k) + R_{2,i} f_i(k), \quad (59)$$

$$z(k) = E_\infty x(k), \quad (60)$$

where x , y , w , and f_i are as previously discussed. **The robust fault detection problem** is to generate a set robust residual signals $r(k)$ that satisfy

$$\|r(k)\|_p \leq J_{th} \text{ if } f_i(k) = 0, \quad (61)$$

$$\|r(k)\|_p > J_{th} \text{ if } f_i(k) \neq 0, \quad (62)$$

where $\|\cdot\|_p$ denotes the p norm of a Lebesgue signal and J_{th} is the i^{th} threshold value. If

¹It would be more desirable to make a lower bound on \mathcal{J}_{rf} large. Unfortunately, lower bounds are usually much more difficult to work with computationally than upper bounds.

the filters (8) are applied to (58)-(59) and E_∞ is chosen as C , (44) can be written as

$$r(k) = Pz(k) + PD_2w_\infty(k) + PR_{2,i}f_i(k). \quad (63)$$

As derived in,¹⁸ if $f_i(k) = 0$ (63) satisfies the norm inequality

$$\begin{aligned} \|r\|_{(\infty,2),[N_0,N]}^2 &\leq \{[\text{tr}(PE_aQ_{a,w}E_a^T P^T)^q]^{\frac{1}{q}} + 2\sigma_{\max}(PD_2)[\text{tr}(PE_aQ_{a,w}E_a^T P^T)^q]^{\frac{1}{2q}} \\ &\quad + \sigma_{\max}^2(PD_2)\} \|\tilde{w}\|_{(\infty,2),[N_0,N]}^2, \end{aligned} \quad (64)$$

where $Q_{a,w}$ is previously defined. The threshold can be chosen as

$$\begin{aligned} J_{th} &\triangleq \{[\text{tr}(PE_aQ_{a,w}E_a^T P^T)^q]^{\frac{1}{q}} + 2\sigma_{\max}(PD_2)[\text{tr}(PE_aQ_{a,w}E_a^T P^T)^q]^{\frac{1}{2q}} \\ &\quad + \sigma_{\max}^2(PD_2)\} \|\tilde{w}\|_{(\infty,2),[N_0,N]}^2. \end{aligned} \quad (65)$$

Robust fault detection can be accomplished by comparing $\|r\|_{(\infty,2),[N_0,N]}$ with J_{th} . A fault occurs if $\|r\|_{(\infty,2),[N_0,N]} > J_{th}$, i.e.,

$$\|r\|_{(\infty,2),[N_0,N]} > J_{th} \Rightarrow \text{a fault occurred.} \quad (66)$$

Optimization Using a Real-Coded Genetic Algorithm

As previously discussed, the design of robust FDI estimators is formulated as an optimization problem. A real-coded genetic algorithm (RCGA) is used to search for a solution. Genetic algorithms (GAs) can efficiently search in complex and possibly discontinuous solution spaces without problem reformulation or evaluation of each solution candidate. They offer the following additional advantages over traditional methods: (1) information about derivatives, Hessians or step sizes is not required, (2) a population of points in the solution space is searched in parallel rather than point by point, and (3) a number of potential solutions to a given problem can be provided. GAs have been proven to provide efficiency (i.e. faster computation times and smaller storage) and flexibility (i.e. adaptation to a range of complex problems) in comparison to traditional methods of optimization. The use of RCGAs, where operations are performed with real numbers, rather than binary GAs, where binary digits are used, proves to be more advantageous. Because no coding or decoding of binary numbers is necessary a subsequent decrease in computational time and storage size is achieved.

An RCGA begins with an arbitrarily chosen initial population within the search region. The algorithm then follows three general operations: (1) *selection*, (2) *recombination*, and (3) *mutation*.³³⁻³⁶ The flowchart for a single population RCGA is shown in Figure 2.

Selection. A common selection process in RCGAs is conducted using stochastic universal sampling.³⁵ Individuals of a population are mapped to a line segment, such that each individual's segment is equal in size to its normalized fitness value. Then, N equally spaced pointers are placed along the line segment, where N is the number of individuals to be selected. The position of the first pointer is determined by a randomly generated number $p \in [0, \frac{1}{N}]$ where $\frac{1}{N}$ is the spacing between pointers. This method of selection is analogous to roulette wheel selection³⁴ and is illustrated in Figure 3 for a population of 8 individuals, n_i , with $N = 4$. From this example it can be seen that individuals n_2, n_3, n_5 and n_7 are chosen.

Recombination. In an RCGA recombination is parallel to crossover in a binary GA. It is the process by which new chromosomes are produced from existing ones and involves the exchange of the individuals' numeric values (genes).^{35,36} Let p_1 and p_2 represent two individuals (parents) who are to reproduce. The offspring p'_1 and p'_2 are produced as a linear combination of the parents:

$$p'_1 = \alpha p_1 + (1 - \alpha)p_2, \quad (67)$$

$$p'_2 = (1 - \alpha)p_1 + \alpha p_2, \quad (68)$$

where $\alpha \in [0, 1]$ is a recombination parameter.

Mutation. The mutation process was originally developed for binary representation. However, other methods have been developed to allow gene modification in an RCGA. The mutation operation randomly alters one or more genes of a selected chromosome. More specifically, randomly generated values are added to the genes with low probability. The probability of mutation is inversely proportional to the number of variables (dimensions). The more dimensions an individual has, the smaller the mutation probability.³⁵ An effective mutation operator, which produces small step sizes with a high probability and large step sizes with a low probability, is defined as

$$Gen_i^{mut} = Gen_i + s_i r_i a_i, \quad i \in \{1, 2, \dots, m\} \text{ uniform at random} \quad (69)$$

$$s_i \in \{-1, +1\}, \quad \text{uniform at random} \quad (70)$$

$$a_i = 2^{-uk}, \quad u \in [0, 1], \quad \text{uniform at random} \quad (71)$$

where s , r , and a are direction, mutation range, and relative step size, respectively, and m is the number of genes in the chromosome. The mutation range is defined in terms of the domain of the genes, and the step size is defined in terms of the mutation precision k .

For the robust ℓ_1 optimization problem the chromosome is constructed by formulating

matrices A_e , W , P , H and N into a single vector Θ such that

$$\Theta = \left[\text{Vec}(A_e)^T \text{Vec}(W)^T \text{Vec}(P)^T \text{diag}(H)^T \text{diag}(N)^T \right]. \quad (72)$$

The search region is then defined by establishing upper and lower limits $\bar{\Theta}$ and $\underline{\Theta}$ such that

$$\underline{\theta}_{ij} \leq \theta_{ij} \leq \bar{\theta}_{ij}. \quad (73)$$

To account for the stability criteria, the RCGA is formulated as a constrained optimization problem. This is achieved by imposing a constraint on the cost with a penalty function. Specifically, if the stability criterion is not satisfied, a multiplicative penalty is imposed on the cost such that

$$\text{if } \begin{cases} \max[\lambda_i(A_a)] < 1, & \mathcal{J} = \mathcal{J} \\ \text{otherwise,} & \mathcal{J} = \text{penalty} * \mathcal{J} \end{cases} \quad (74)$$

where λ_i , $i \in (1, 2, \dots, m + 2n)$ are the eigenvalues of the augmented system A_a . Using this type of penalty helps to insure that, because of fitness values, individuals representing unstable systems will not survive the selection process. The penalty is chosen as 100 such that the unstable fitness values will be two orders of magnitude larger than their true values.

Illustrative Example of FDI for a Jet Engine

A numerical example is presented in this section to illustrate robust ℓ_1 estimator design using the Popov-Tsytkin multiplier and the application of the robust ℓ_1 estimator to robust fault detection of dynamic systems. The model used was supplied by NASA Glenn Research Center and is given as

$$x(k+1) = (A + \Delta A)x(k) + Bu(k) + D_{\infty,1}w_{\infty}(k) + R_a f_a(k), \quad (75)$$

$$y(k) = (C + \Delta C)x(k) + Du(k) + D_{\infty,2}w_{\infty}(k) + R_s f_s(k) \quad (76)$$

where the sampling period $T_s = 0.01$ sec. Only sensor faults are considered in this example, thus $R_a = 0$. The elements of the state vector $x \in \mathcal{R}^3$, are

$x_1 \triangleq$ High Pressure Spool Speed (rpm)

$x_2 \triangleq$ Low Pressure Spool Speed (rpm)

$x_3 \triangleq$ High Pressure Compressor Inlet Temperature ($^{\circ}C$).

The elements of the control input vector $u \in \mathcal{R}^3$, are

$$\begin{aligned} u_1 &\triangleq \text{Main Burner Fuel Flow (kg/hr)} \\ u_2 &\triangleq \text{Exhaust Nozzle Throat Area (m}^2\text{)} \\ u_3 &\triangleq \text{Bypass Duct Area (m}^2\text{)}. \end{aligned}$$

The elements of the output vector $y \in \mathcal{R}^3$, are

$$\begin{aligned} y_1 &\triangleq \text{Corrected High Pressure Spool Speed (rpm)} \\ y_2 &\triangleq \text{Corrected Low Pressure Spool Speed (rpm)} \\ y_3 &\triangleq \text{Corrected High Pressure Compressor Inlet Temperature (}^\circ\text{C)}. \end{aligned}$$

The variable w denotes a vector of disturbance signals.

The uncertainty matrices, ΔA and ΔC , are representative of some engine degradation over time. Thus, it is assumed that a newly constructed engine can be modeled with the nominal matrices A and C and with use, the parameters of the degraded engine are encompassed in the uncertainty. The system parameter matrices are

$$A = \begin{bmatrix} 0.9835 & 0.0110 & 0.0039 \\ 3.788e-4 & 0.9858 & 0.0026 \\ 4.230e-6 & -2.282e-4 & 0.9891 \end{bmatrix}, \quad D_{\infty,1} = \text{diag}\{0.1, 0.1, 0.01\}, \quad (77)$$

$$B = \begin{bmatrix} 0.0080 & 0.2397 & -0.0383 \\ 0.0068 & 0.1565 & 0.0248 \\ 2.691e-4 & -2.912e-4 & 2.558e-4 \end{bmatrix}, \quad R_s = \begin{bmatrix} 1 & 0 & 0 \\ 0 & 1 & 0 \\ 0 & 0 & 1 \end{bmatrix}, \quad (78)$$

$$C = \begin{bmatrix} 0.2383 & 0.4871 & 0.1390 \\ -1.074e-5 & -8.399e-4 & 3.784e-4 \\ 2.070e-5 & -4.132e-5 & -4.335e-6 \end{bmatrix}, \quad (79)$$

$$D = \begin{bmatrix} 0.4171 & -4.492 & 0.4875 \\ 7.968e-4 & -0.0050 & 2.861e-4 \\ -1.270e-5 & 4.837e-4 & -0.0021 \end{bmatrix}, \quad D_{\infty,2} = 0.1 \times I_{3 \times 3}. \quad (80)$$

The uncertainty matrices $\Delta A = -H_A F_A G_A$ and $\Delta C = -H_C F_C G_C$, where

$$\begin{aligned} H_A &= - \begin{bmatrix} 1 & 0 & 0 \\ 0 & 1 & 0 \\ 0 & 0 & 1 \end{bmatrix}, \quad H_C = - \begin{bmatrix} 1 & 1 & 1 \\ 0 & 0 & 0 \\ 0 & 0 & 0 \end{bmatrix}, \\ G_A &= \begin{bmatrix} I_{3 \times 3} \end{bmatrix}, \quad G_C = \begin{bmatrix} I_{3 \times 3} \end{bmatrix}, \\ F_A &= \text{diag}\{\delta_{A_1}, \delta_{A_2}, \delta_{A_3}\}, \quad F_C = \text{diag}\{\delta_{C_1}, \delta_{C_2}, \delta_{C_3}\}, \end{aligned} \quad (81)$$

with

$$\begin{aligned} -0.02167 &\leq \delta_{A_1} \leq 0.02167, & -0.02174 &\leq \delta_{A_2} \leq 0.02174, \\ -0.02181 &\leq \delta_{A_3} \leq 0.02181, \end{aligned} \quad (82)$$

$$\begin{aligned} -0.01787 &\leq \delta_{C_1} \leq 0.01787, & -0.03653 &\leq \delta_{C_2} \leq 0.03653, \\ -0.01043 &\leq \delta_{C_3} \leq 0.01043. \end{aligned} \quad (83)$$

Note that the uncertain parameters $\delta_{A_1} \dots \delta_{A_3}$ correspond to parameter fluctuations in the diagonal elements of matrix A and $\delta_{C_1} \dots \delta_{C_3}$ correspond to the first row of C . In the real-coded genetic algorithm, the chromosome string Θ (72) consisted of 39 genes, corresponding to the elements of $A_e \in \mathcal{R}^3$, $W \in \mathcal{R}^3$, $P \in \mathcal{R}^3$ and the diagonal elements of H , $N \in \mathcal{D}^6$. By using the objective function (57) with stability constraints (74), the respective gain and projection matrices are obtained for a bank of estimators. The nominal (uncertainty not considered) gain matrices were

$$W_{n,1} = \begin{bmatrix} -4.3677 & 0.9652 & 2.1343 \\ -46.331 & -0.4433 & 2.5012 \\ 185.10 & 0.0755 & -12.637 \end{bmatrix}, \quad P_{n,1} = \begin{bmatrix} 0.0324 & -0.1080 & 1.7946 \\ -0.0042 & 0.0218 & -0.0179 \\ 0.0242 & -0.0931 & 1.3789 \end{bmatrix}, \quad (84)$$

$$W_{n,2} = \begin{bmatrix} 8.5628 & 2.1809 & -0.9584 \\ -12.065 & 4.3910 & 1.2877 \\ 34.830 & 0.6572 & -3.4886 \end{bmatrix}, \quad P_{n,2} = \begin{bmatrix} -0.0072 & 0.3017 & 0.2845 \\ 0.0009 & -0.0376 & -0.1761 \\ 0.0092 & -0.3725 & -1.8386 \end{bmatrix}, \quad (85)$$

$$W_{n,3} = \begin{bmatrix} 11.665 & 2.2105 & -11.263 \\ -6.0256 & -1.1449 & -17.177 \\ 5.0019 & 0.9603 & -17.767 \end{bmatrix}, \quad P_{n,3} = \begin{bmatrix} -0.0041 & 0.3916 & -0.9689 \\ 0.0005 & -0.0207 & -0.2238 \\ -0.0025 & 0.3185 & -1.8625 \end{bmatrix}. \quad (86)$$

Note for all nominal filters the system matrix $A_e = A$. The robust (uncertainty explicitly

considered) gain matrices obtained were

$$W_{r,1} = \begin{bmatrix} 0.0445 & 3.0049 & -0.0722 \\ -1.1029 & -0.7468 & 0.0282 \\ 12.8499 & 0.0867 & -0.1242 \end{bmatrix}, P_{r,1} = \begin{bmatrix} 0.0235 & 0.0430 & -0.2387 \\ -0.0072 & 0.2216 & 0.0108 \\ -0.0066 & -0.0337 & 0.0567 \end{bmatrix}, \quad (87)$$

$$A_{e,1} = \begin{bmatrix} 0.9049 & 0.0109 & 0.0040 \\ 0.0004 & 0.7968 & 0.0025 \\ 3.789e-6 & -0.0002 & 1.0687 \end{bmatrix}, \quad (88)$$

$$W_{r,2} = \begin{bmatrix} -0.0218 & 0.5019 & -0.0161 \\ 0.1665 & -250.65 & 0.0066 \\ 6.7877 & 0.0019 & -0.0030 \end{bmatrix}, \quad (89)$$

$$P_{r,2} = \begin{bmatrix} -4.143e-7 & 0.2373 & -2.0956 \\ -4.423e-7 & 0.0012 & 0.0062 \\ -2.894e-6 & -8.729e-5 & -0.0011 \end{bmatrix}, \quad (90)$$

$$A_{e,2} = \begin{bmatrix} 0.5480 & 0.0021 & -0.0003 \\ -1.057e-5 & 0.8245 & -0.0063 \\ 9.35980069e-6 & -0.0013 & 2.4357 \end{bmatrix}, \quad (91)$$

$$W_{r,3} = \begin{bmatrix} 9.1728 & 9.5942 & -1.8998 \\ -1.1983 & -3.0317 & -221.94 \\ -0.4734 & 0.7084 & -127.55 \end{bmatrix}, P_{r,3} = \begin{bmatrix} -0.0047 & 0.4759 & -0.3249 \\ -5.4336 & 0.0421 & -0.0067 \\ 0.0027 & -0.6124 & 1.36088 \end{bmatrix}, \quad (92)$$

$$A_{e,3} = \begin{bmatrix} 0.4731 & 0.0192 & 0.0075 \\ 0.0035 & 0.0955 & 5.180e-5 \\ -3.203e-6 & -1.691e-5 & 0.2037 \end{bmatrix}. \quad (93)$$

As shown above, for both the nominal and robust systems three filters were designed corresponding to targeted faults f_1 , f_2 and f_3 . To verify the solutions obtained by the RCGA, the frequency response of the closed-loop systems were examined. Specifically, Bode diagrams were used to check the magnitude of the transfer functions from the faults f_1 , f_2 , and f_3 , and the disturbances w_1 , w_2 and w_3 to the residual signals r_1 , r_2 and r_3 . Figure 4 shows the response of filter 3 of the nominal system, where the target fault is f_3 and the residual signal is r_3 . It can be seen that the influence of the target fault signal on the residual is significantly larger than the influence of the nuisance faults and disturbances over all frequencies. Similarly, in Figure 5 filter 2 of the robust system, where the target fault is f_2 and the residual signal is r_2 , the influence of the target fault signal on the residual is

larger than the nuisance faults and disturbance signals.²

In order to illustrate the application of the robust ℓ_1 estimator to robust fault detection, FDI of the system in (75) and (76) subject to plant disturbances was performed. A bank of estimators (as described in Section 3) was designed for the set of y_i , $i \in \{1, 2, 3\}$, sensor outputs, i.e., the i^{th} estimator is designed to detect a fault in the y_i sensor while neglecting faults in the remaining sensors. Here the nominal case as well as the robust case are considered for the FDI process. Random white noise signals with zero mean were added as both the disturbance inputs and sensor noise. The variances of the disturbance inputs, w_1 , w_2 and w_3 , were 0.05, 0.08 and 0.03, respectively. In order to show the extent of robustness, uncertainty for all system matrices was considered. The uncertain parameters are assigned random values within their respective ranges. The values are given in Table 1.

This example only considered the occurrence of sensor faults within the system. A typical sensor fault in the jet engine is a drift in the sensor reading. Thus, a slow drifting (or ramping) sensor fault was added to a sensor reading at a particular instant in time. Specifically, the simulated fault signal can be described by the linear function

$$f_i(k) = \begin{cases} 0, & k < k_f \\ \tau(k - k_f), & k \geq k_f \end{cases} \quad (94)$$

where $\tau = 0.1$ is the slope and k_f is the instant at which the fault occurs. Due to the disturbance the finite-horizon infinity norm (64) of the residual with $N - N_0 = 60$ (corresponding to a time interval of 0.6 sec.), was nonzero even in the absence of faults.

In Figures 6 through 8 a single sensor fault was introduced in the system. Specifically, in Figure 6 a fault was introduced in sensor y_1 at $t = 20$ sec, Figure 7 has a fault introduced in sensor y_2 at $t = 30$ sec, while a fault in sensor y_3 is introduced at $t = 40$ sec in Figure 8. It can be seen that both the nominal and robust estimators were able to successfully detect and isolate each fault. This is evident as each faulty sensor the residual surpassed its respective threshold at the the time of occurrence of each fault. However, it is noted that in each nominal estimator system false alarms are given in one of the fault free sensors. This is due to the fact that uncertainty was not accounted for in the design of these estimators. These false alarms are avoided with the robust filters. In Figure 9 multiple faults were introduced in sensors y_1 , y_2 and y_3 at $t = 25$ sec, $t = 10$ sec and $t = 40$ sec, respectively. It can be observed that in this instant both nominal and robust systems were able to isolate each target fault from the other nuisance faults. A false alarm is again given as the first residual surpasses its threshold well before a fault is introduced in the sensor. This does not occur

²These trends are representative of the behavior of each filter response.

with the robust estimator.

Conclusions

This paper considered the application of robust ℓ_1 estimation for uncertain, linear discrete-time systems to the robust fault detection and isolation. Mixed structured singular value theory of¹⁸ was used to design a bank of robust ℓ_1 estimators and the resulting fixed threshold logic. By considering a discrete, linear model of a jet engine with real parametric uncertainties and introducing drifting sensor faults, it was shown that the robust FDI methodology based on fixed thresholds was capable of detecting and isolating failures in each of the particular sensors. Also, by designing the robust estimators to explicitly account for uncertainty false alarm rates were significantly reduced.

References

- ¹Chen, J. and Patton, R. J., "A robust study of model-based fault detection for jet engine systems," *IEEE Proceedings-Control Theory and Applications*, July 1992, pp. 871-876.
- ²"Special Section on Supervision, Fault Detection and Diagnosis of Technical Systems," *Control Engineering Practice*, Vol. 5, No. 5, May 1997.
- ³Frank, P. M., "Fault diagnosis in dynamic systems using analytical and knowledge - based redundancy - A survey and some new results," *Automatica*, Vol. 26, No. 3, 1990, pp. 459-474.
- ⁴Frank, P. M. and Ding, X., "Survey of robust residual generation and evaluation methods in observer-based fault detection systems," *Journal of Process Control*, Vol. 7, No. 6, 1997, pp. 403-424.
- ⁵Gertler, J. J., "Survey of Model-Based Failure Detection and Isolation in Complex Plants: Survey and Synthesis," *IEEE Control Systems Magazine*, 1988, pp. 3-11.
- ⁶Gertler, J. J., "Analytical Redundancy Methods in Fault Detection and Isolation," *IFAC Symposium on Fault Detection, Supervision and Safety for Technical Processes*, 1991, pp. 9-21, Baden-Baden-Germany.
- ⁷Patton, R. J., "Robust Model-Based Fault Diagnosis: The State of the Art," *IFAC Symposium on Fault Detection, Supervision and Safety for Technical Processes*, 1994, pp. 1-24, Espoo-Finland.
- ⁸Patton, R. J. and Chen, J., "A Survey of Robustness Problems in Quantitative Model-Based Fault Diagnosis," *Applied Mathematics and Computational Science*, Vol. 3, No. 3, 1993, pp. 399-416.
- ⁹Gertler, J. J., "Fault detection and isolation using parity relations," *Control Engineering Practice*, Vol. 5, 1997, pp. 653-661.

¹⁰Niemann, H. H. and Stoustrup, J., "Filter design for fault detection and isolation in the presence of modeling errors and disturbances," *Proceedings of IEEE Conference on Decision and Control*, December 1996, pp. 1155–1160, Kobe–Japan.

¹¹Collins, E. G. and Song, T., "Robust H_2 estimation with application to robust fault detection," *Journal of Guidance, Control and Dynamics*, Vol. 23, No. 6, 2000, pp. 1067–1071.

¹²Willsky, A. S., Chow, E. Y., Gershwin, S. B., Greene, C. S., Houpt, P. K., and Kurkjian, A. L., "Dynamic Model-Based Techniques for the Detection of Incidents on Freeways," *IEEE Transactions on Automatic Control*, Vol. AC-25, June 1980, pp. 347–360.

¹³Willsky, A. S. and Jones, H. L., "A Generalized Likelihood Ratio Approach to the Detection and Estimation of Jumps in Linear Systems," *IEEE Transactions on Automatic Control*, Vol. AC-21, February 1976, pp. 108–112.

¹⁴Collins, E. G. and Song, T., "Multiplier-based robust H_∞ estimation with applications to robust fault detection," *Journal of Guidance, Control and Dynamics*, Vol. 23, No. 5, 2000, pp. 857–864.

¹⁵Edelmayer, A., Boker, J., and Keviczky, L., " H_∞ Detection Filter Design for Linear Systems: Comparison of Two Approaches," *Proceedings of the IFAC 13th Triennial World Congress*, 1996, pp. 37–42, San Francisco–California.

¹⁶Qiu, Z. and Gertler, J. J., "Robust FDI Systems and H_∞ -Optimization," *Proceedings of IEEE Conference on Decision and Control*, December 1993, pp. 1710–1715, San Antonio–Texas.

¹⁷Ajbar, H. and Kantor, J. C., "An ℓ_∞ approach to robust control and fault detection," *Proceedings of the American Control Conference*, June 1993, pp. 3197–3201, San Francisco–California.

¹⁸Collins, E. G. and Song, T., "Robust ℓ_1 estimation using the Popov-Tsympkin multiplier with applications to robust fault detection," *International Journal of Control*, Vol. 74, No. 3, 2001, pp. 303–313.

¹⁹Faitakis, Y. E. and Kantor, J. C., "Residual generation and fault detection for discrete-time systems using an ℓ_∞ technique," *International Journal of Control*, Vol. 64, No. 1, 1996, pp. 155–174.

²⁰Curry, T., Collins, E. G., and Selekwa, M., "Robust Fault Detection Using Robust ℓ_1 Estimation and Fuzzy Logic," *Proceedings of the American Control Conference*, June 2001, pp. 1753–1758, Washington, D.C.

²¹Collins, E. G., Haddad, W. M., Chellaboina, V., and Song, T., "Robustness Analysis in the Delta-Domain Using Fixed-Structured Multipliers," *Proceedings of IEEE Conference on Decision and Control*, December 1997, pp. 3286–3291, San Diego–California.

²²Fan, M. K. H., Tits, A. L., and Doyle, J. C., "Robustness in the Presence of Mixed Parametric Uncertainty and Unmodeled Dynamics," *IEEE Transactions on Automatic Control*, Vol. 36, No. 1, January 1991, pp. 25–38.

²³Haddad, W. M. and Bernstein, D. S., "Parameter-Dependent Lyapunov Functions and the Popov Criterion in Robust Analysis and Synthesis," *IEEE Transactions on Automatic Control*, Vol. 40, 1995, pp. 536–543.

²⁴Haddad, W. M., Bernstein, D. S., and Chellaboina, V.-S., "Generalized Mixed- μ Bounds for Real and Complex Multiple-Block Uncertainty with Internal Matrix Structure," *International Journal of Control*, Vol. 64, 1996, pp. 789–806.

²⁵Theodor, Y. and Shaked, U., "Robust Discrete-Time Minimum-Variance Filtering," *IEEE Transactions on Signal Processing*, Vol. 44, 1996, pp. 181–189.

²⁶Xie, L., Soh, Y. C., and Souza, C. E., "Robust Kalman Filtering for Uncertain Discrete-Time Systems," *IEEE Transactions on Automatic Control*, Vol. 39, 1994, pp. 1310–1314.

²⁷Xie, L., Souza, C. E., and Fun, M., " H_∞ Estimation for Discrete-Time Linear Uncertain Systems," *International Journal of Robust and Nonlinear Control*, Vol. 1, 1991, pp. 111–123.

²⁸Blanchini, F. and Sznajder, M., "Rational ℓ_1 suboptimal compensators for continuous-time systems," *IEEE Transactions on Automatic Control*, Vol. 39, 1994, pp. 1487–1492.

²⁹Haddad, W. M. and Chellaboina, V.-S., "Mixed-Norm H_2/ℓ_1 Controller Synthesis via Fixed-Order Dynamic Compensation: A Riccati Equation Approach," *Proceedings of IEEE Conference on Decision and Control*, December 1997, pp. 452–457, San Diego-California.

³⁰Elia, N. and Dahleh, M. A., *Computational Methods for Controller Design*, Springer-Verlag, London, 1998.

³¹Haddad, W. M. and Kapila, V., "Discrete-time extensions of mixed- μ bounds to monotonic and odd monotonic nonlinearities," *International Journal of Control*, Vol. 61, No. 2, 1995, pp. 423–441.

³²Commault, C., Dion, J. M., Sename, O., and Motyeian, R., "Observer-based fault detection and isolation for structured systems," *IEEE Transactions on Automatic Control*, Vol. 47, No. 12, 2002, pp. 2074–2079.

³³Davis, L., *Handbook of Genetic Algorithms*, Van Nostrand Reinhold, New York, 1991.

³⁴Goldberg, D., *Genetic Algorithms in Search, Optimization and Machine Learning*, Addison-Wesley, Massachusetts, 1989.

³⁵Pohlheim, H., *Tutorial: Genetic and Evolutionary Algorithm Toolbox for use with Matlab*, Matlab toolbox documentation, 1999.

³⁶Wright, A. H., "Genetic algorithms for real parameter optimization," *Foundations of*

Genetic Algorithms, 1991, pp. 205–218, Rawlins, G., Ed., Morgan Kaufmann Publishers,
Los Altos.

List of Table Captions

Table 1: Uncertain Parameter Values

	Figure 6	Figure 7	Figure 8	Figure 9
δ_{A_1}	0.004217	-0.000386	0.003415	-0.010360
δ_{A_2}	-0.011812	-0.007753	-0.009804	-0.007485
δ_{A_3}	0.007793	0.003931	0.006159	-0.000564
δ_{C_1}	0	-0.010086	-0.012755	-0.009738
δ_{C_2}	0	0.011859	0.018581	-0.001702
δ_{C_3}	0	-0.000169	0.001494	-0.004532

List of Figure Captions

Figure 1: Estimation Based Fault Detection and Isolation

Figure 2: Flow chart of single population RCGA

Figure 3: Stochastic universal sampling for real-coded selection

Figure 4: Frequency Response: Nominal Filter 3 - target fault f_3 and residual signal r_3

Figure 5: Frequency Response: Robust Filter 2 - target fault f_2 and residual signal r_2

Figure 6: Robust ℓ_1 FDI: fault in y_1 sensor at $t = 20$ sec.

Figure 7: Robust ℓ_1 FDI: fault in y_2 sensor at $t = 30$ sec.

Figure 8: Robust ℓ_1 FDI: fault in y_3 sensor at $t = 40$ sec.

Figure 9: Robust ℓ_1 FDI: fault in y_1 at $t = 25$ sec., y_2 at $t = 10$ sec., and y_3 sensor at $t = 40$ sec.

